Published in final edited form as:
Eur J Neurosci. 2013 January ; 37(1): 63–79. doi:10.1111/ejn.12021.

Nonassociative Plasticity Alters Competitive Interactions Among Mixture Components In Early Olfactory Processing

Fernando F Locatelli[1,2], **Patricia C Fernandez**[1,3], **Francis Villareal**[1], **Kerem Muezzinoglu**[4], **Ramon Huerta**[4], **C. Giovanni Galizia**[5], and **Brian H. Smith**[1]

[1]School of Life Sciences, Arizona State University, P.O. Box 874501, Tempe, AZ 85287

[4]Biocircuits Institute, University of California, San Diego, La Jolla, CA 92093-0328

[5]University of Konstanz, Department of Biology, D-78457 Konstanz, Germany

Abstract

Experience related plasticity is an essential component of networks involved in early olfactory processing. However, the mechanisms and functions of plasticity in these neural networks are not well understood. We studied nonassociative plasticity by evaluating responses to two pure odors (A and X) and their binary mixture using calcium imaging of odor elicited activity in output neurons of the honey bee antennal lobe. Unreinforced exposure to A or X produced no change in the neural response elicited by the pure odors. However, exposure to one odor (e.g. A) caused the response to the mixture to become more similar to the other component (X). We also show in behavioral analyses that unreinforced exposure to A caused the mixture to become perceptually more similar to X. These results suggest that nonassociative plasticity modifies neural networks in such a way that it affects local competitive interactions among mixture components. We used a computational model to evaluate the most likely targets for modification. Hebbian modification of synapses from inhibitory local interneurons to projection neurons most reliably produces the observed shift in response to the mixture. These results are consistent with a model in which the antennal lobe acts to filter olfactory information according to its relevance for performing a particular task.

Keywords

Olfaction; learning; antennal lobe; plasticity; *Apis mellifera*

Introduction

Animals must be able to perceptually filter out stimuli that are not relevant for survival. In general, infrequent stimuli are more informative than stimuli that are common (Shannon, 1948). For example, when faced with regular exposure to a stimulus that is not associated with an important consequence, such as food or a painful stimulus, animals typically decrease responsiveness to that stimulus. The decrease is defined as ‘habituation’ when the

Corresponding author: Brian H. Smith, School of Life Sciences, Arizona State University, P.O. Box 874501, Tempe, AZ 85287. brian.h.smith@asu.edu.
[2]Present address: Laboratorio de Neurobiología de la Memoria, Departamento de Fisiología, Biología Molecular y Celular, Facultad de Ciencias Exactas y Naturales, Universidad de Buenos Aires, IFIByNE (UBA CONICET), Ciudad Universitaria, 1428EHA Buenos Aires, Argentina.
[3]Present address: INTA, EEA Delta del Paraná, (UBA CONICET), Rio Paraná de las Palmas y Canal Comas, 2804, Campana, Argentina

None of the authors have a conflict of interest for this work.

behavioral response to the stimulus is innate and the decrease can be not explained by motor fatigue. For example, rats and mice investigate a new odor at first, but the intensity of investigation wanes with repeated exposure (Hunter and Murray, 1989; Cleland et al., 2002). Fruit flies show innate avoidance behavior to certain odors, but the behavior habituates after massive, sustained exposure (Das et al., 2011). A related case of nonassociative learning is latent inhibition (Lubow, 1973). In contrast to habituation, animals are repeatedly exposed to a stimulus that does not at first elicit a behavioral response. Latent inhibition becomes evident only when the preexposed stimulus is subsequently associated with reinforcement in conditions that usually produce a robust conditioned response. For example, after regular exposure to an odor honey bees are slow to develop a conditioned response to that odor relative to other odors (Chandra et al., 2010).

The neural mechanisms that underlie olfactory nonassociative learning and memory have received relatively less attention than the mechanisms for pavlovian and operant conditioning. Yet there is indication that the mechanisms for nonassociative learning are complex and distributed in the brain. In mammals, components of this plasticity can be found in early olfactory processing in the olfactory bulb and piriform cortex (Wilson and Linster, 2008). At least part of the neural mechanism responsible for short-term olfactory habituation lies in a homosynaptic depression of transmission from second-order mitral cells in the olfactory bulb to their targets in the piriform cortex, and it depends on glutamate receptors on axon terminals of the mitral cells (Linster et al., 2009). Prolonged or repeated exposure to odor produces habituation that depends on NMDA receptors in the olfactory bulb network (Wilson and Linster, 2008).

Neural networks involved in early olfactory processing are functionally similar in insects and mammals (Hildebrand and Shepherd, 1997; Strausfeld and Hildebrand, 1999). Furthermore, this similarity is most likely due to convergent evolution (Strausfeld and Hildebrand, 1999), which indicates that these neural networks reflect fundamental and broadly applicable solutions for olfactory encoding and plasticity. However, this similarity remains to be thoroughly investigated, particularly in regard to different types of plasticity. Here we investigate whether odor exposure that is sufficient to produce latent inhibition in the honey bee induces nonassociative modification of the the neural networks in the antennal lobe, which is the functional analog to the mammalian olfactory bulb. Using calcium imaging, we show that after regular presentation of an odor the neural representation of that odor is reduced in its ability to compete with that of a new odor when both are presented in a mixture. This result implies that network-level interactions in the antennal lobe are modified by unreinforced exposure. Furthermore, we show that this competition is reflected in behavioral overshadowing experiments. Finally, we use a computational model of the AL to predict specific synaptic changes that modify competitive interactions in the network with the same results as observed experimentally. Among the three conceivable hypotheses tested, the simplest one, namely Hebbian plasticity on inhibitory synapses towards the excitatory units, is the most likely mechanism.

Materials and Methods

Animals

Honey bee (*Apis mellifera carnica*) pollen foragers (all female) were collected at the entrance of the colony, shortly cooled and restrained into individual Plexiglas stages suited for olfactory conditioning and optical recordings (Galizia and Vetter, 2004). After recovery from cooling, bees were fed 2 μl of a 1.0 M sucrose solution and remained undisturbed until staining or until further feeding. All imaging or behavior experiments were performed one day after capturing and restraining the animals.

Projection neuron staining

The head was fixed to the Plexiglas stage with soft dental wax (Kerr, Sybron Dental Specialties, USA) in a way that animals could freely move antennae and proboscis. A rectangular window was cut in the head capsule dorsal to the joints of the antennae and ventral to the medial ocellus. The glands were carefully moved aside until the alpha-lobes in the brain were visible, which are easily recognizable and serve as spatial reference to guide staining. Projection neurons (PNs) were stained by backfilling with the calcium sensor dye FURA-dextran (potassium salt, 10.000 MW, Invitrogen, Eugene, OR). The tip of a glass electrode was coated with a bolus (approx 50μm diameter) of fura-dextran prepared in 3% bovine serum albumin solution (Sigma-Aldrich, St Louis, MA). The coated electrode was inserted into both sides of the protocerebrum dorsolateral to the alpha-lobes where the antenno-protocerebral tracts (APTs) run between the median and lateral calyxes of the mushroom bodies (Kirschner et al., 2006). Median- and lateral-ACTs contain the axons of uniglomerular PNs (Abel et al 2001). The dye bolus dissolved into the tissue in 3 to 5 seconds and the window was immediately closed using the same piece of cuticle that was previously removed. Eicosane was used to glue and seal the cuticle. Twenty minutes after staining the bees were fed again until satiation with 1 M sucrose and left undisturbed until next day. The dye was left to travel along the tracts for at least 12 h. Before imaging, the antennae were fixed pointing towards the front using eicosane (Sigma-Aldrich) and body movements were prevented by gently compressing the abdomen and thorax with a piece of foam. The brain was rinsed with Ringer solution (130 mM NaCl, 6 mM KCl, 4 mM MgCl2, 5 mM CaCl2, 160 mM sucrose, 25 mM glucose, 10 mM HEPES, pH 6.7, 500 mOsmol; all chemicals from Sigma-Aldrich, St Louis MA) and glands and trachea covering the antennal lobes were removed. The antennal lobes were examined for appropriate staining and only animals that by visual inspection presented homogenous staining of all visually accessible glomeruli were used for experiments. To prevent brain movements during measurements, a second hole was cut ventrally to the antennae and the compact structure of muscles, esophagus, and supporting chitin was lifted and put under slight tension (Mauelshagen, 1993). Finally, the brain was covered with Kwik-sil (WPI) to further prevent movements and avoid desiccation during the experiment. After surgery animals were mounted in the microscope and were allowed to recover for 20 min before imaging.

Imaging

Calcium imaging was done using a CCD camera (SensiCamQE, T.I.L.L. Photonics, Germany) mounted on an upright fluorescence microscope (Olympus BX-50WI, Japan) equipped with a 20× dip objective, NA = 0.95 (Olympus), 505 DRLPXR dichroic mirror and 515 nm LP filter (TILL Photonics, Germany). Monochromatic excitation light provided by a PolichromeV (TILL Photonics), alternated between 340 and 380 nm. Fluorescence was detected at a sampling rate of 5 Hz. Spatial resolution was 172 ×130 pixels binned on chip from 1,376 × 1,040 pixels, resulting in a spatial sampling of 2.6 μm per pixel side. Exposure times were 8 and 2 ms for 340 and 380 nm excitation light, respectively.

Animals underwent four imaging sessions, with an odor exposure session between the first and second imaging sessions (Fig. 2A). Each imaging session included six measurements of odor-induced activity in the antennal lobe: 2 measurements each of 1-hexanol, 2-octanone and the binary mixture 1:1. The six measurements were presented in random order and were separated by 1 minute intervals. Ten minutes after the end of the first imaging session animals underwent an odor exposure session that lasted 40 minutes. The exposure session consisted of 40 unrewarded stimulations with 1-hexanol or 2-octanone. Odor stimulations lasted 4 seconds and the inter-trial interval was 1 min. Three complete imaging sessions were repeated 10, 40 and 70 minutes after the end of the exposure session. The two

measurements of each odor within each session were used to test for reliability of signals and were further averaged during analysis.

Imaging analysis

Image analysis was done using software written in IDL (Research systems, CO, USA) by Giovanni Galizia and Mathias Ditzen (Routines can be requested from the authors). Each measurement consisted of a double sequence of 50 fluorescence images obtained at 340 nm and 380 nm excitation light (Fi_{340}, Fi_{380}, where i is the number of the image from 1 to 50). For each pair of images Fi we calculated pixel-wise the ratio $Ri = (Fi_{340nm} / Fi_{380nm}) \times 100$ and subtracted the background ratio Rb, obtained by averaging the Ri values 1 s immediately before the odor onset [$Rb = 1/8 (R_{10} + \ldots + R_{14})$]. Resulting values, shown in the figure as ΔR, represent the change from the reference window and are proportional to the changes in the intracellular calcium concentration. Quantitative analysis of odor-induced activity patterns was based on calcium signals in identified glomeruli. For this aim, glomeruli were identified on the basis of their morphology and relative position using the digital atlas of the honey bee AL as a reference (Galizia et al., 1999). The visualization of glomeruli was possible by observing the raw fluorescence images obtained at 380nm excitation light, and we additionally used software written by Mathias Ditzen that allows clear view of glomerular shape and position. The software calculates images representing the degree of correlation between neighboring pixels. Since glomeruli respond as functional units, pixels stemming from the same glomerulus are highly correlated over time. In contrast, pixels from different glomeruli are uncorrelated. This provides images in which glomeruli are visible and clearly separated by contrasting boundaries. Figures 1A shows examples of raw and correlation images used for glomeruli identification. Eighteen glomeruli could be unequivocally identified across all animals and thus were used for the present analysis. All glomeruli are located in the dorso-rostral side of the AL. We examined activity in glomeruli 17, 23, 24, 25, 28, 29, 33, 35, 36, 37, 38, 42, 43, 47, 48, 49, 52 that belong to tract 1 from the antennal nerve and glomerulus 45 from tract 3 according to the nomenclature previously established (Galizia et al., 1999; Flanagan and Mercer, 1989). Glomerular activation was calculated by averaging activity in a square area of 9×9 pixels that correspond to 23.4 × 23.4 μm and fits well within the boundaries of the glomeruli. Glomerular activity in the present study refers to activity of the uniglomerular PNs that innervate the selected glomeruli.

Principal component analysis

Odor induced activity patterns were characterized in the present study by measuring calcium signals in 18 identified glomeruli of the dorsal side of the AL. Therefore, each data point, i.e. each odor at each time point, is described by an 18 dimensional vector. We performed Principal Component Analysis (SPSS Inc.) to ease visualization of the different activity patterns evoked by the three odors and also to show evolution of the patterns across time. The data set was reorganized as a single 2D-matrix composed by the three odors and all time-points (frames) between 600 ms before odor onset and 2000 ms after odor offset as rows and 18 glomeruli as columns (Example of a data point: 1-hexanol/at 500ms: glom17, glom23,…,glom52). This matrix was subjected to PCA and varimax rotation. The 2 first principal components explain 92% of variance in this example and clearly separate 1-hexanol, 2-octanone and the mixture. The data set of all 1-hexanol exposed bees and all 2-octanone exposed bees were correspondingly averaged to get two ‘average-bees’ (see methods in Fernandez et al., 2009): the 1-hexanol bee and the 2-octanone bee, resp. Each of the two average-bees have data points that corresponded to the three odors at each time point of the measurement and at four sessions (before exposure, 10, 40 and 70 min after exposure). The data sets corresponding to the average bees were organized in a 2D-matrix, configured with each data point (odor/session/frame) as rows and 18 glomeruli as columns

(example of one data point: 1-hexanol/10min-session/at 500ms: glom 17; glom 23;……..; glom 52). The matrix was subjected to PCA and Varimax rotation to reduce the 18 dimensions. The 2 first PCs explain 97 and 95 % of variance in the groups of bees exposed to 2-octanone and 1-hexanol respectively. Note that PCA performed on data from the average bees is used only for mere visualization of the effect, while analysis and conclusions are strictly based on correlation analysis as it is explained in the next section.

Pattern similarity assessment

Odor-elicited patterns are represented as vectors with 18 elements and each element constitutes the glomerular activity averaged during 1 second of odor stimulation. Euclidean distances or correlation coefficients are normally valid parameters used to evaluate similarity between patterns. However, the accuracy of both parameters as predictors of perceptual similarity between two odors might change depending on features of the odors that are to be compared. In a preliminary analysis we compared the outcome of both parameters for the three possible comparisons: i.e. 1-hexanol vs. 2-octanone; 1-hexanol vs. mixture; and 2-octanone vs. mixture. For the odors, concentrations and mixture compositions used in the present work, Pearson correlation coefficient was a better predictor of the perceptual similarity than the Euclidean Distances. Thus, throughout this study we used the Pearson correlation coefficient as measure of similarity between the activity patterns evoked by two odors in the same animal and during the same session. In order to analyze whether the unrewarded exposure session biases the representation of the mixture towards or away from the representation of the components, we calculated the correlation coefficients between the mixture and the pure components for each bee and each session. Subsequently, the correlation values were categorized according to the odor used in the exposure session. Statistical analysis was based on a 2-way repeated measures ANOVA and contrasts between all post-exposure sessions and the pre-exposure session. For ANOVA, correlation values were grouped as exposed-mixture or as novel-mixture. Sessions were considered as repeated factor for statistical analysis. No significant difference was found between sessions, neither for the exposed or the novel odors as separate factors. However, the interaction term and interaction contrasts between the pre-exposure session and the post-exposures sessions were statistically significant.

Electroantennogram

Electroantennogram recordings were performed to test for a possible decrement in olfactory input after exposure training. Honey bees were caught, restrained in Plexiglas holders and fed following the same procedure described for the imaging experiments. The head was fixed to the holder with wax and a 25 μm uninsulated silver wire was inserted into the right eye and used as ground electrode during recordings. The position of the antennae was fixed with eicosane and the tip of the left antenna was cleanly cut. A glass microelectrode filled with a 0.1M KCl solution mounted on a WPI electrode adapter was inserted through the open tip of the antenna. The EAG signal was fed into a DAM50 Bio-Amplifier (WPI). The output was digitalized with an analog-digital converter (Lab-Trax 4, WPI) and recorded for offline data analysis (Data-Trax 2, WPI). Stimulation conditions, odor concentration, stimulus duration and odor sequence were identical to those used for imaging experiments. Only two recording sessions were performed that corresponded to the first and second sessions of the imaging experiments. Both sessions were separated by 60 min. The 1st session finished 10 min before starting the 40 min exposure session and the 2nd recording session started ten min after the end of the exposure session. The exposure session that followed was identical to the exposure session for the imaging experiment. Amplitude of odor-induced signals was calculated by subtracting the potential recorded before odor onset. All of the analyses were based on the average of two measurements per odor and per

session. Statistical analysis was based on 2-way repeated measures ANOVA with odor as an independent factor (novel odor/exposed odor /mixture) and sessions as a repeated factor.

Behavior

Honey bees were exposed to an odor and later conditioned to a mixture that contains that odor in order to measure if exposure affects learning performance to the mixture. Animals were captured, restrained and fed following the same procedures used in imaging and EAG experiments. One day after capture, animals were divided into three groups. Two groups underwent an exposure session identical to the exposure session used in imaging experiments. The exposure session lasted 40 min and consisted in 40 4-sec unrewarded stimulations with 1-hexanol or 2-octanone. A blank group was manipulated in the same way but received only clean air during the whole exposure session. Fifteen minutes after the end of the exposure session all groups were subjected to olfactory conditioning of the proboscis extension reflex (Bitterman et al., 1983), during which all animals were identically conditioned to a 1:1 mixture of 1-hexanol and 2-octanone over three trials. During conditioning animals received a sucrose reward three sec after odor onset. Reward consisted of first touching the antennae with a 2.0 M sucrose-water solution, which elicited proboscis extension, and followed by feeding with 0.4 μl. The inter-trial interval was 10 minutes. Fifteen minutes after the end of the conditioning session, the conditioned response was assessed in a test session using 1-hexanol or 2-octanone. Each animal was tested only once. Proboscis extension was recorded as a binary variable – proboscis extension or not - during the training and test trials. Extension of the proboscis beyond the virtual line between the open mandibles during odor presentation was effectively counted as proboscis extension. On acquisition trials, the response was determined for each subject as positive if the subject extended its proboscis during odor stimulation and before the US presentation. These data are plotted as the percentage of subjects that responded to the mixture on each trial during training or to the single odors during test trials.

Odor stimulation

Odors used for stimulation were the aliphatic alcohol 1-hexanol and the ketone 2-octanone (both TCI America, Portland OR 98%), alone or combined in binary mixtures 1:1. Odors were diluted from purity 1/100 or 1/10 in mineral oil (M-8410, Sigma-Aldrich, St. Louis, MO) for imaging or behavior experiments. The output of the odor delivery device, for both behavioral or imaging experiments, was positioned 2 cm away from the animal's head and the air stream was aimed toward the antennae. During the periods without odor stimulation a continuous charcoal filtered air stream (25 ml/sec) ventilated airspace around the antennae. A constant exhaust removed odors from the arena. The odor cartridges consisted of a 1 ml glass syringe containing a filter paper strip (0.5 × 8 cm) loaded either with 5 μl 1-hexanol solution + 5 μl mineral oil, 5 μl 2-octanone solution + 5 μl mineral oil; or 5 μl 1-hexanol solution + 5 μl 2-octanone solution. Three-way valves (LFAA1200118H; The LEE Company, Essex, CT) controlled the onset of the airflow through the odor cartridge. When the valve was open, the air inside the cartridges was pushed into the continuous air stream in a mixing chamber 2 cm before the output of the odor delivery device. During behavior experiments, opening and closing of the valves was triggered by a programmable controller (Automation-Direct) and the odor duration was 4 sec. During imaging experiments, the opening of the valve was synchronized with the optical recordings by the imaging acquisition software TILLVision (TILL Photonics, Germany). In an earlier study (Fernandez et al., 2009) we found that odor durations of 600ms or longer leads to odor recognition independent of the duration of stimulations. This allowed us to reduce the odor stimulation during the imaging sessions to only one second and shorten the whole duration of the imaging protocol. This shortening is important since the UV light (340 and 380 nm) needed for the calcium imaging recordings is targeted to the animals brain and long exposures lead

to cell damage by phototoxicity. The odor delivery device had eight independent and identical channels, each of them composed by a valve attached to an odor cartridge. Between experiments, odors were rotated to balance possible differences between channels.

Conductance based model

The model network consists of 20PNs and 20LNs wired according to the generative model shown in Fig 6A. The basic structure of the model (Bazhenov et al., 2001) is used with some modifications to better account for the calcium current. The LNs receive input from ORNs, other LNs and PNs (Wilson et al., 2004; Distler et al., 1998). The PNs integrate the incoming ORNs and LNs activity as well as the sparse input from other PNs. The membrane potential V_{PN} of each PN and LN is modeled by the differential equation

$$C_m \frac{dV_{\mathrm{PN/LN}}}{dt} = -g \cdot (V_{\mathrm{PN/LN}} - E) - I_{\mathrm{Na}} - I_{\mathrm{K}} - I_{\mathrm{Ca}} - I_{\mathrm{KCa}} - I_{\mathrm{syn}} - I_{\mathrm{stim}}$$

where the reversal potential was E=55mV, the membrane capacitance was C_m=0.1nF, and the membrane conductance was g=0.04μS. Note that LN in the honeybee are spiking neurons in contrast to the LNs of the locust antennal lobe.

Intrinsic currents

I_{Na}, I_{K} are described by $I_X = g_X n^N h^M (V_{\mathrm{PN/LN}} - E_X)$ with the gating variables n and h evolving according to $dn/dt = (n_\infty(V_{\mathrm{PN/LN}}) - n)/\tau_n(V_{\mathrm{PN/LN}})$ and $dh/dt = (h_\infty(V_{\mathrm{PN/LN}}) - h)/\tau_h(V_{\mathrm{PN/LN}})$, both within the interval [0,1]. For the fast sodium current I_{Na}, the parameters were g_{Na}=5μS, N=3, M=1, E_{Na}=50mV, $\tau_n = 3/(\alpha_n(V_{\mathrm{PN/LN}}) + \beta_n(V_{\mathrm{PN/LN}}))$, $n_\infty = \alpha_n(V_{\mathrm{PN/LN}})/(\alpha_n(V_{\mathrm{PN/LN}}) + \beta_n(V_{\mathrm{PN/LN}}))$, $\tau_h = 3/(\alpha_h(V_{\mathrm{PN/LN}}) + \beta_h(V_{\mathrm{PN/LN}}))$, and $h_\infty = \alpha_h(V_{\mathrm{PN/LN}})/(\alpha_h(V_{\mathrm{PN/LN}}) + \beta_h(V_{\mathrm{PN/LN}}))$, where, $\alpha_n(V_{\mathrm{PN/LN}}) = -0.32 \cdot (V_{\mathrm{PN/LN}} + 42)/(e^{-0.25 \cdot (42 + V_{\mathrm{PN/LN}})} - 1)$, $\beta_n(V_{\mathrm{PN/LN}}) = 0.28 \cdot (V_{\mathrm{PN/LN}} + 15)/(e^{-0.2 \cdot (V_{\mathrm{PN/LN}} + 15)} - 1)$, $\alpha_h(V_{\mathrm{PN/LN}}) = 0.128 \cdot e^{-(38 + V_{\mathrm{PN/LN}})/18}$, and $\beta_h(V_{\mathrm{PN/LN}}) = 4/(e^{-0.2 \cdot (15 + V_{\mathrm{PN/LN}})} + 1$. For the fast potassium current I_{K}, the parameters were g_{K}=1μS, N=4, M=0, E_{K}=−95mV, $\tau_n = 3/(\alpha_n(V_{\mathrm{PN/LN}}) + \beta_n(V_{\mathrm{PN/LN}}))$, $n_\infty = \alpha_n(V_{\mathrm{PN/LN}})/(\alpha_n(V_{\mathrm{PN/LN}}) + \beta_n(V_{\mathrm{PN/LN}}))$, where $\alpha_n(V_{\mathrm{PN/LN}}) = -0.32 \cdot (V_{\mathrm{PN/LN}} + 30)/(e^{-0.2 \cdot (V_{\mathrm{PN/LN}} + 30)} - 1)$ and $\beta_n(V_{\mathrm{PN/LN}}) = 0.5 \cdot e^{-(V_{\mathrm{PN/LN}} + 35)/40}$. The intrinsic calcium current is described using the Goldman-Hodgkin-Katz formalism due to the large differences in calcium concentration between inside and outside the cell. If we assume that the calcium differences are always large we can write $I_{\mathrm{Ca}} = 0.2 n^3 h V_{\mathrm{PN/LN}}/(1 - e^{2 V_{\mathrm{PN/LN}}/24.42})$ (Huerta et al., 2000; Szucs et al., 2009) where the gating variables n and h satisfied the differential equations above with the parameters $\tau_h = 20 - 19{,}9/(1 + e^{(V_{\mathrm{PN/LN}} - 40.1)/8})$, $n_\infty = 1/(1 + e^{(-V_{\mathrm{PN/LN}} - 27.1)/7.18})$, $\tau_h = 30 + 100/(1 + e^{(V_{\mathrm{PN/LN}} + 50.1)/5})$, and $h_\infty = 1/(1 + e^{(V_{\mathrm{PN/LN}} + 27)/3.5})$.

The calcium dependent potassium current was modeled by $I_{\mathrm{KCa}} = 0.15(V_{\mathrm{PN/LN}} + 95)\left([\mathrm{Ca}]^4/\left([\mathrm{Ca}]^4 + K_{\mathrm{Ca}}^4\right)\right)$, where K_{Ca}=0.5μM. Here, [Ca] denotes the calcium concentration, which is described by a first order kinetic equation as follows $d[\mathrm{Ca}]/dt = 0.001(4I_{\mathrm{Ca}} - 0.42[\mathrm{Ca}] + 0.1)$. To stay consistent with the experimental calcium measurements, the read-out from the PN was made through the calcium concentration.

Synaptic currents

The stimulus current I_{stim} to i-th PN was considered as a current pulse of the ORN that the PN is attached to (as shown in the Fig. 6A). The synaptic current into i-th PN was the sum of currents from adjacent inhibitory LNs. For each adjacent LN j, the synaptic current was described by $I_{\mathrm{syn}}^j = g_i^j \left(V_{\mathrm{PN}}^i + 80\right) / \left(1 + e^{(0.5 - V_{\mathrm{LN}}^j)/7}\right)$, where g_i^j is the conductance associated with

the synapse from the *j*-th LN to the current (*i*-th) PN, and V_{LN}^{j} is the membrane potential of the *j*-th LN. For each excitatory synapse (arriving from the *j*-th PN), the synaptic current component was described by $I_{\mathrm{syn}}^{j}=g_i^j r\,(V+70mV)$, where g_i^j denotes the conductance of the synapse (now arriving from *j*-th PN) and *r* is the bound receptor state, which is subject to the dynamics $dr/dt = \alpha \cdot [T](1 - r) - \beta \cdot r$ as proposed in Destexhe et al. (1994). Here, [*T*] denotes the transmitter concentration in the form of a pulse, that is [*T*]=1μ*M* within the first 2 seconds following a spike in the pre-synaptic PN, and [*T*]=0, otherwise. The rise and decay constants α and β were selected as 10^{-4} ms^{-1}μM^{-1} and $2\cdot10^{-4}$ ms^{-1}μM^{-1}, respectively.

Firing Rate model

A firing rate model was used to concentrate on the role of the synaptic transmission without taking into effect the intrinsic dynamics of the neurons. The rate model is used since it allows more effective evaluation of what aspects of the connectivity and its plasticity are relevant to explain a given phenomena. As rate model we use the well known Wilson-Cowan rate model (Wilson & Cowan, 1972). This simple model consists of N_{PN} excitatory PNs, and N_{LN} inhibitory LNs, units whose activities evolved according to

$$\frac{dx_i}{dt}=\Theta\left(-\sum_{j=1}^{N_{LN}} w_{ij}^{EI}\cdot y_j+E_i(S)\right), i=1,\ldots,N_{PN},$$

$$\frac{dy_i}{dt}=\Theta\left(\sum_{j=1}^{N_{PN}} w_{ij}^{IE}\cdot x_j-\sum_{j=1}^{N_{LN}} w_{ij}^{II}\cdot y_j+I_i(S)\right), i=1,\ldots,N_{LN},$$

respectively. Here Θ(·) denotes the piecewise linear activation function. The connectivity and conductance values were generated by a Bernoulli process, which assigned to each element of the matrices $\mathbf{W}^{EI}$ the value 1.0 with probability 0.5 independently, or zero otherwise. The second connectivity matrix $\mathbf{W}^{IE}$ was generated in the same way for the conductance value 0.5. $\mathbf{W}^{II}$ was set with probability of 0.4 and conductance of 0.5. The stimulus was injected to the network through the PNs with $E_i(S)$ and LNs using the term $I_i(S)$. This function generates an arbitrary pulse value of 5 for the pure odor A and for the pure odor B, reaching a different subset of PNs for different odors (note that the arbitrary value does not change the results). It is set to zero when there is no odor present at the input.

Synaptic Plasticity

The firing rate model and the conductance based model were used to test three different hypotheses of synaptic plasticity that may account for the changes observed in the representation of the mixtures: they were: **a)** plasticity in synapses from LNs to PNs; **b)** from PNs to LNs; and **c)** from LNs to LNs. If the observed changes cannot be reproduced using simple models and basic plasticity rules, then the mechanisms of synaptic plasticity that we propose may not be sufficiently general. In this regard, note that the model's dynamics is driven by intrinsic elements of the AL network and direct inputs from the ORNs. The model does not consider feedback from other brain regions (Hu et al., 2010; Kirschner et al., 2006; Rybak & Menzel 1993), and it does not consider modulatory inputs (Hammer 1997) that are needed for associative learning.

RESULTS

Odor exposure changes competition between components in a mixture

Our previous analyses of nonassociative olfactory conditioning in honey bees have shown that twenty or more presentations of an odor without reinforcement, at 30 sec or 5 min intervals, delays subsequent learning of an association of that odor with sucrose reward (Chandra et al., 2010). We set out to evaluate whether the neural basis for this nonassociative conditioning, or at least a component of it, might reside in the first synaptic relay for olfaction in the brain – the antennal lobe. We employed a well-established method for using a calcium indicator to backfill axons of the Projection Neurons that innervate identified glomeruli on the dorsal surface in the AL (Fig. 1A; (Sachse and Galizia, 2002). This method has revealed robust odor-specific spatio-temporal activity patterns that reflect differential activation of PNs during and shortly after odor stimulation (Fig. 1B–1E; Galan et al., 2006; Fernandez et al., 2009). These 'transients' define a sequence of activity patterns across glomeruli of the AL. The activation of glomeruli changes from one time point to the next, and the identity of the odor can be defined by the identity of the activated glomeruli, their relative activation and the sequence of states in the transient. Mixing two pure odorants produces a graded change in activity that is proportional to the mixture (Fernandez et al., 2009). Binary mixtures that are biased toward one component (e.g. 9:1 or 7:3) are statistically more similar to the dominant component. Furthermore, differentially reinforcing two mixtures increases the separation of the transients for those mixtures (Fernandez et al., 2009), which indicates that associative plasticity influences odor representations in the AL.

We chose two odors (1-hexanol and 2-octanone) used in our previous analysis of plasticity in the AL (Fernandez et al., 2009) because they elicit distinct but slightly overlapping activity patterns (Fig. 1B–1D; (Sachse et al., 1999)). A 1:1 mixture elicits an activity pattern that is intermediate to the components. Using Principal Components Analysis to reduce the number of dimensions from 18 to 2, we plotted this activity over 200 ms time steps from shortly before odor presentation through several steps after termination of the stimulus (Fig. 1E shows transient patterns from a single animal). The pattern of activity through time produces a transient through this two dimensional space that projects out and begins to return before the odor is terminated (Fdez Galán et al., 2004; Fernandez et al., 2009; Mazor and Laurent, 2005). The Euclidian distance between corresponding time points across the transients reaches a maximum approximately 400–600 ms after odor onset (Fernandez et al., 2009). From background activity near the origin, the transients for the two pure odors run approximately parallel to each axis, whereas the transient for the mixture projects at an angle intermediate to the other transients (Fig 1E and Fernandez et al., 2009). The similarities between the patterns elicited by the pure odorants and the mixture are reflected in the Pearson correlation values between the glomerular activity patterns (Fig. 1D, 1F). Each pure odorant is more similar to the mixture than the pure odorants are to each other. Figure 1F averages the correlation coefficient for the three odor pairs obtained for 17 animals (different letters indicate significant differences by LSD contrasts $P < 0.01$ after significant ANOVA: $F_{2,48} = 19.49$, $P < 0.0001$).

Our experiments included four identical imaging sessions (Fig. 2A). The first imaging session occurred prior to exposure treatment and was used to establish the AL response patterns prior to training. Then we presented animals with 40 unreinforced exposures to an odorant. This treatment is sufficient to decrease the probability that the odor will elicit a conditioned response when associated with reinforcement (Chandra et al., 2010). The exposure treatment was followed by three additional test series performed 10, 40 and 70 min after the end of the exposure treatment. We could then compare the responses among the pure odorants and the mixture during each of the four test sessions.

Unreinforced exposure changed the way the AL network processes odors. The most dramatic effect was a shift in the transient for the mixture (Fig. 2B). After exposure to a pure odor, the transient for the mixture shifted away from that odor and toward the pure odor that was not exposed. The effect was the same for exposure to 1-hexanol (left panel) and 2-octanone (right panel).

This noticeable shift in the trajectory of the transients is reflected in the change in the correlation between each pure odor and the mixture. Figures 3A and 3B show the actual correlation values between pure odors and the mixture before (bold diamonds) and after (small diamonds) exposure for each animal. The correlation between a pure odor and the mixture is variable from animal to animal before exposure treatment. However, after exposure the response to the mixture became more correlated to the novel (not exposed) odor in 12 of 17 animals (Fig 3A). Furthermore, the mixture became less correlated to the exposed odor (Fig 3B) in 13 of 17 animals. The mean change (+/− SE) across animals in the correlation between the mixture and the two odors (novel and exposed) is shown in Fig. 3C. At all three post-exposure test times the novel odor became more similar to the mixture and the exposed odor became less similar. Statistical analysis was based on the raw correlation values presented in figure 3A and B. For two way ANOVA we considered “Odor condition” (novel or exposed) as one factor, and “Session” as the second and repeated factor. No significant effect was found neither for odor condition ($F_{1,32} = 0.222$, NS) nor for session ($F_{3,96} = 0.378$, NS); however the interaction term was highly significant ($F_{3,96} = 6.351$, $P = 0.001$). All interaction contrasts comparing pre-exposure measurements vs. post-exposure measurements were significant: pre vs. post10’ ($F_{1,32} = 5.075$, $P = 0.04$); pre vs. post40’ ($F_{1,32} = 10.292$, $P = 0.003$); pre vs. post70’ ($F_{1,32} = 12.038$, $P = 0.002$).

The change in the mixture representation is not a consequence of sensory adaptation

In order to evaluate if the changes that we observe have arisen from adaptation of sensory receptors on the antennae, we performed the following additional analysis and experiments. First, we calculated the global antennal lobe response for each odor as the sum of the activity elicited in all glomeruli (Fig. 4A). The rationale behind this analysis is that if sensitivity to a mixture component is reduced as a consequence of sensory adaptation, then PN activity should reflect the input reduction as though a lower odor concentration had been presented (Sachse and Galizia, 2003). A reduction in signal because of sensory adaptation should therefore be pronounced for the odor used for unreinforced exposure. Since no differences were found for 1-hexanol or 2-octanone exposed bees, the data for the exposed odor, novel odor and mixture were pooled. Figure 4A shows the global response in the antennal lobe across four sessions. The data were not normalized to avoid occlusion of changes between sessions. Instead, the data are shown as absolute values of the sum of calcium responses in all measured glomeruli. There was no detectable reduction in the global antennal lobe activity for the exposed odor that would arise from sensory adaptation. The statistical analysis based on two way ANOVA with “Odor“ as one factor and ”Session” as the repeated factor showed a significant effect for odor ($F_{2;63} = 6.6$ $P < 0.01$). These significant result is based on significant differences among the activity elicited by the mixture vs. pure odors (Tukey-HSD contrasts $P < 0.05$ in both cases), and not between pure odors ($P = 0.98$). This stronger response to the mixture is consistent with the fact that the activity elicited by the mixture involves the sum of glomeruli activated independently by each pure odor, as has been previously shown using imaging techniques that reflect activity in sensory neurons (Joerges et al. 1997; Deisig et al. 2006) or in projection neurons (Deisig et al., 2010). Differences among sessions were statistically significant (session factor: $F_{3:189} = 5.02$, $P < 0.01$). Tukey-HSD contrasts showed significant differences between the first and the third, and between the first and the fourth session ($P < 0.05$ in both cases). The increase in activity across sessions is independent of the odor and not consistent with sensory

adaptation. Finally, the interaction term was not significant ($F_{6:189} = 0.08$, $P = 0.99$) revealing that the observed changes along sessions were independent of the treatment.

Second, we performed electroantennogram measurements to directly measure summed afferent activity from sensory neurons into the antennal lobe. We performed two recording sessions that corresponded to the first and second session of the imaging experiments (Fig 4B). The first recording session finished ten minutes before the exposure protocol. A group of 5 bees was exposed to 1-hexanol and a second group of 5 bees was exposed to 2-octanone. The second recording session was performed 10 min after the end of the exposure protocol. If sensory adaptation was responsible for the results reported in the previous sections, then the adaptation should clearly be expressed during this session. Since there was no difference between both groups of bees, and the amplitude of EAG signals evoked by 1-hexanol and 2-octanone were similar, we regrouped the data from 1-hexanol and 2-octanone treated bees into novel, exposed or mixture odor, as we did in the previous experiments. No change was observed 10 min after the end of the exposure for any of the odors (mixture, novel or exposed odors; figure 4B). Statistical analysis based on two way ANOVA with "Odor" as one factor and "Session" as repeated factor revealed no effect of the main factors or for the interaction; session factor ($F_{1:27} = 0.52$, NS); odor factor (novel, exposed or mixture, $F_{2:27} = 3.18$, NS) and interaction term ($F_{2:27} = 0.43$, NS). The tendency to a stronger response obtained by stimulation with the mixture (figure 4B) is consistent with more sensory neurons recruited under this condition.

Finally, the level of the response measured during the second session may have been the sum of two separate effects; one related to the odor exposure and another related to the 60 min gap between sessions. Therefore as a control in a separate set of animals we measured the responses during both sessions without exposing the animals to any treatment during the 60 min interval (figure 4C). Two-way ANOVA with "Odor (pure or mixture)" as one factor and "Session" as repeated factor revealed no effect neither for the main factors nor for the interaction term (odor: $F_{1:13} = 1.01$, NS; session: $F_{1:13} = 0.14$, NS; interaction term $F_{1:13} = 0.03$, NS).

In summary, both the global activity and EAG experiments failed to provide evidence of reduced sensory input for the exposed odor that could provide an alternative account for the shift observed in the representation of the mixture after exposure.

A novel odor more easily overshadows an exposed odor

The imaging data indicate that the mixture became perceptually more similar to the novel odor as a result of exposure. Therefore, a novel odor should be more capable of overshadowing a preexposed odor in a behavioral test. We tested this possibility using a Proboscis Extension Response conditioning procedure for restrained honey bees (Fig. 5A; Bitterman et al., 1983). Three groups of bees underwent exposure protocols of 40 unreinforced presentations at 1 min inter-stimulus intervals, as in the exposure treatments used in the previous sections. One group was exposed to 1-hexanol; another group was exposed to 2-octanone and a third group was exposed to clean air as control. Most odors elicit PER with a low probability on the first trial (ca 10% of honey bees show a response prior to associative conditioning). The genesis of these spontaneous responses is still not well understood (Smith et al. 2006). But this probability is low and equivalent across odors we selected and treatment groups in our study. Furthermore, these responses completely disappear after 40 preexposures (Chandra et al. 2010). Therefore, we did not record PER during the unreinforced exposure. We followed the unreinforced exposure with three conditioning trials during which the 1:1 mixture was reinforced with sucrose in a way that produces robust conditioned responding to the odor. Statistical analysis of performance during conditioning was based on two way repeated measures ANOVA: "Trial" as the

repeated factor showed the significant effect of training ($F_{2,266} = 73$, $P < 0.0001$), the "group" factor and the "interaction term" were not significant ($F_{1,133} = 0.39$ and $F_{4,266} = 0.7$, respectively). Thus, honey bees in all three groups learned to respond equally well to the mixture (Fig. 5B).

Finally, after conditioning to the mixture we tested the response to each pure odor to evaluate the perceptual similarity of the mixture to the components. The responses to pure odors during the test depended on the exposure treatment. Honey bees responded equally to each of the pure odors after exposure to air (Fig. 5C, middle), which is the typical result for these odors in this protocol. This response after mixture conditioning is typically lower than after conditioning to the pure odor (Smith, 1998), which indicates overshadowing. However, overshadowing is symmetric for animals that were pre-exposed to clean air. In contrast, exposure to odor prior to mixture conditioning caused overshadowing to become asymmetric. After exposure to 1-hexanol, the strongest response occurred to 2-octanone after mixture conditioning (Fig. 5C, left). In contrast, the strongest response occurred to 1-hexanol after exposure to 2-octanone (Fig. 5C, right). In figure 5D the data obtained during testing is shown and analyzed independently of the odor identity and only based on the condition of the odor in the mixture: i.e. exposed odor; novel odor (for an odor accompanying an exposed odor) or any odor in case of the blank group.

Overall, the response to an odor after conditioning to a binary mixture containing that odor depended significantly on whether or not animals had been exposed to that odor without reinforcement (Fig. 5D; left column). Moreover, the response to a novel odor combined in a mixture with an exposed odor was enhanced (Fig. 5D, right column). Kruskal-Wallis test showed statistical differences among responses elicited by the three odor conditions shown in figure 5D ($F_{2,133} = 3.13$, $P < 0.05$). Further statistical analysis using pair-wise Chi^2 comparisons showed significant differences only between the novel and the exposed condition ($P = 0.014$). The observation that learning scores for odors of the novel and the exposed condition are not statistically different from the learning scores for odors in the blank group but they are different from each other, suggests a mechanism that biases learning of the novel and the exposed odor in opposite directions. In summary, this shift in the perceptually dominant component of the mixture toward the new odor is consistent with the imaging data.

LN to PN connections are the most likely targets for nonassociative plasticity

The imaging data and the resulting change in perception of the mixture imply an alteration in competitive interactions within the AL network. We used a well-established conductance-based model of transient dynamic coding in the insect AL (Bazhenov et al., 2001) and a rate model (Huerta and Rabinovich 2004) to explore which synapses might be the most likely targets for future investigation. The network consisted of two clusters of 20 inhibitory local interneurons (LNs) and 20 PNs (Fig. 6A). The odor inputs are modeled by injecting current to a particular set of PNs for odor A and another set of PNs for odor X. The level of overlap between both PN groups was varied from 1 to 5 PNs in order to simulate odor pairs with different degrees of overlap. Each LN receives inputs in a nonselective manner. In order to be consistent with the imaging data, the activity of PNs was monitored by the level of calcium set by the term ICa in the model (see Methods).

For consistency with the imaging experiments, the model employed a pretraining phase in which we used the initial network as it was generated by a Bernoulli process (Huerta and Rabinovich 2004). The 20-dimensional PN (calcium) responses were recorded for pure odors A, X and the mixture. Plasticity was not applied at any synapse in this phase. We adopt the stimulation protocol used in the imaging experiments: the pure odor A, the pure odor X and the mixture (A+X) were applied sequentially to the network in a random order.

These stimuli were encoded in a 20-dimensional binary vector with its entries denoting the presence or absence of the pure odors at the input. In each presentation, the network was stimulated with its corresponding PN activation group for 2 seconds and relaxed for the following 5 seconds until the onset of the next stimulation. This phase of the simulation allowed us to generate the 20-dimensional calcium trajectories representing the three types of stimuli and to form the principal component space where we carried out the analysis.

In the training phase, the synaptic efficacy of a subset of LN-to-PN synapses was modified. The synapses affected in each presentation were determined based on the instantaneous network activity. They were potentiated according to the following Hebbian learning rule: increase the conductance associated with all synapses where both the pre-synaptic LNs and the post-synaptic PNs are active (i.e., spiking). This modification was applied to each qualified synapse incrementally for each presentation during the training phase. The increment to the i-th selected synapse was set as 5% of the current conductance value at the onset of the presentation. The potentiation saturated at 150% of the initial conductance of the synapse. In this plasticity scheme, most PN activity saturates within the first 10 presentations of the training odor. Note, however, that the applied plasticity progressively reduces the total excitation across the LN population, which in turn may reduce the total inhibition to the PN population. Therefore, the training time required for the synaptic connections to reach the bound and stabilize may be longer. For that reason we have kept the network in the training phase for 20 presentations, although the changes in the affected synaptic conductances vanished well before the end of training presentations due to the imposed 150% limit. In the post-training phase, we fixed the synaptic conductances in the network and tested the network once again in random order with the pure odors A and X and the binary mixture.

Fig. 6C shows the projected calcium trajectories in each phase of the experiment and for both training odors. The thick loops correspond to the presentations of odor A, X, and the mixture during the intial phase before training. In each graph, the three thin loops in blue and red color correspond to the three representations of pure A and pure X during training and in the post-training phase. The three thin green loops show the trajectory for the mixture at the 5th and 15th training trial and at the post-training phase in the order indicated by the arrow. Notice that the initial trajectories for the mixture may look different and shifted from the middle of the PC space in both figures even though they represent the pre-training state of the same network. The different shapes are due to different runs on separate PCAs for visualization of the shift provoked by treatment.

We simulated 100 random networks generated independently using the connectivity shown in Fig. 6A. The average increment in a LN-to-PN synapse modified by odor exposure over all tested networks was relatively large (0.0373 μS). As in the imaging experiments (Fig. 3C), the correlation between the mixture and the odor that was not exposed increased across trials (Fig. 6B). Exposure to either odor shifted the response to the mixture toward the novel (not exposed) odor (Fig. 6C, D). The increase in the correlation between the mixture and the novel odor was measured along 100 samples placed uniformly on the respective loops.

A successful AL network is defined as one that demonstrates a significant increase in such correlation, namely a 10% increase with respect to pre-training correlation. The correlation between two distinct network responses is calculated as follows: First, for each PN, the single-channel time series for the two stimuli are recorded during the exposure period. Then, the cross-correlation between such pair of signals is obtained. The maximum correlation value over a range of time lags between the time series is extracted as a similarity measure between the pairs of recorded signals. Finally, the correlations obtained for each pair of individual PN responses in this way are added up and interpreted as the correlation between

the two multi-dimensional PN responses. Out of 100 random realizations of the model, 98 of them demonstrated such an increase after the training phase, making them successful in reproducing the imaging data. The magnitude of potentiation during training trials and the saturation level regarding the synaptic conductances were tuned to maximize this success rate.

The total inhibition originating from LN activity into the PN population is the key quantity in this phenomenon (Fig. 7 for an example of exposure to odor A). The total inhibition is strictly larger when the mixture (i.e., both odors A and X together) stimulates the network than when only odor A or X stimulate the network. By construction with the given parameters, the A-type PNs are initialized just above their firing thresholds. Upon training with odor A, the total inhibition onto A-type PNs is increased and most of these units turn silent when stimulated with the mixture. On the other hand, the bound introduced on the plasticity (i.e., 1.5 times the original conductance on the affected synapses) ensures that the total inhibition recruited by stimulus A after training is not enough to suppress responses in A-type PNs when stimulated with odor A alone.

We also used a rate model to investigate whether plasticity at specific synapses would be more effective in generating the changes we observed. In addition to the LN to PN plasticity, we tested PN to LN and LN to LN synaptic changes. Out of the 1000 train-test episodes performed on the sample networks for the rules LN-to-PN, PN-to-LN, and LN-to-LN, 98.6%, 76.3%, and 32.4% of the trials were successful, respectively. Based on these results, we included LN-to-PN and PN-to-LN synapses for further analysis with the conductance-based model and ruled out LN-to-LN. In order to test this prediction derived from the rate model we applied synaptic plasticity from the PN to LN in the conductance based model running 100 random realizations. We observed that 78 instances out of 100 random realizations were successful which is consistent with the success rates observed in the rate models. The LN-to-LN model was significantly less successful than LN-to-PN and PN-to-LN to a probability value inferior to 0.001 with a power of 99.99%.

We also reproduced the phenomena by using other hypothetical connections from the ORN into the AL. In particular, we tested the possibility that the LNs do not receive direct input from the ORNs such that they only get activated by the PNs (data not shown). The results also showed that the most effective connections to modulate information filtering were the LN-to-PN connections, which is consistent with the results previously described. It is remarkable that regardless of the network design and stimulus input into the AL, the most effective connections to modulate the information filtering are LN-to-PN.

Discussion

Our analyses are consistent with a model in which plasticity in the AL sets up a filter for processing odors (Smith et al., 2006; Smith, 1996). It is now clear that associative and nonassociative mechanisms of plasticity are essential components of that filter (Faber et al., 1999; Stopfer and Laurent, 1999; Sandoz et al., 2003, Yu et al., 2004; Sachse et al., 2007; Denker et al., 2010; Das et al., 2011; Rath et al., 2011). A major question that remains regards how these mechanisms interact to reshape the way the networks process sensory information. In the AL of the moth *Manduca sexta* (Daly et al., 2004), different types of pairing of odor with sucrose reinforcement restructured the responses to odor in the AL network. Simply pairing odor with sucrose increased excitatory responses in the AL, and presentation of odor alone decreased responses. Differential conditioning of one odor paired with sucrose and the other presented alone produced more complex switches between excitation and inhibition. Although it was clear from this work that both nonassociative and associative plasticity influence the AL network, the function of this plasticity in terms of

coding remained elusive. More recently, similar response changes in PNs of the AL after differential conditioning were reported for the honey bee (Fernandez et al., 2009). This study went on to show that the changes served to increase the separation between the spatiotemporal response patterns for a reinforced versus unreinforced odor, presumably making the odors perceptually more distinct (Sandoz et al., 2003).

Here we have used calcium imaging to reveal that nonassociative mechanisms related to latent inhibition contribute to this separation by changing the competitive interactions between two different spatiotemporal activity patterns. The result is that a novel odor is more clearly represented in a binary mixture when it is combined with a previously unreinforced odor. We also show that these changes in the AL correlate to changes in perceptual properties of the mixture in behavioral experiments. The pair of odors used in the present work was selected because the odors have similar salience when separately used as a conditioned odor (Guerrieri et al., 2005; Fernandez et al., 2009), and neither perceptually dominates the other in behavioral or imaging experiments. Since a 1:1 mixture produces a relatively graded change from either component, we felt that this condition was the best one to begin to look for plasticity-induced changes. Latent inhibition and overshadowing have been shown using several different odors (Smith 1998, Chandra et al 2010), which indicates that our results will broadly apply to many odor pairs. Furthermore, our mathematical modeling also predicts that different degrees of overlap among the components should not affect the present conclusion. Nevertheless, the AL may have built-in or learned asymmetries in the way it processes different odors. Therefore, extension of our behavioral and imaging analyses to compare pairs of odors that have differing degrees of overlap or activation of glomeruli will be important.

The change in correlation among the pure odors and the mixture was very consistent across animals. The representation of the mixture became more similar to the novel odor and less similar to the exposed odor. Moreover, we showed that measuring only a fraction of the glomeruli in the AL, i.e. 18 out of 165, was sufficient to detect changes that correlated with the changes in the behavior. This perhaps surprising result might have two possible explanations. First, the glomeruli that are particularly relevant for this type of learning for these odors could have happened to be among the 18 glomeruli we targeted. That explanation seems less likely because we have not been able to identify single glomeruli that showed a statistically significant change after training, which is consistent with our previous report about plasticity in the AL (Fernandez et al., 2009) as well as with related studies (Peele et al., 2006; Rath et al, 2011; but see Sandoz et al., 2003 and Yu et al., 2004). Alternatively, and perhaps more likely, the plasticity driven by odor exposure may be small and distributed across many glomeruli. In Fernandez et al., 2009 and here we showed that the change in the network is not dominated by one or two glomeruli. Instead, plasticity is reflected in the summation of small changes across many glomeruli. This interpretation seems consistent with the small but significant change reported after analyzing only 18 of the 165 glomeruli that conform the AL. If more glomeruli could be imaged the changes might be more obvious than the ones we report here. Furthermore, it is possible that plasticity affects different glomeruli in different animals such that the changes vanish when glomerular activity is averaged across bees. Variability across animals might be expected given that we used forager bees for the experiments, and each animal could have had its olfactory network shaped by different experiences in the field.

The changes we observed might be related to mechanisms of non-associative plasticity already described in the AL. Protein kinase A is important for nonassociative plasticity in the AL (Müller and Hildebrandt, 2002), and this could be an important mechanism underlying the plasticity at the circuit level that we describe. Also, unreinforced exposure to an odor can increase synchronization among PNs (Stopfer and Laurent, 1999) or induce

odor-specific changes in spontaneous background activity (Galan et al., 2006). However, the latter effects last only a few minutes. In contrast, we show that exposure alters competitive interactions with other odors that lasts up to 70 min, and behaviorally, latent inhibition lasts at least 24 hrs (Chandra et al., 2010). More detailed analyses will be needed to reveal whether these forms of non-associative modification of the AL are related, and that will require a more detailed understanding of the neural mechanisms that underlie them.

As a first step toward investigating the possible underlying neural mechanisms, we have chosen to implement nonassociative plasticity in a well-developed model of the insect AL (Bazhenov et al., 2001). Our modeling efforts performed both with realistic conductance models and mean firing rate models replicated the experimental findings. We found out that the most effective manner to filter out a repetitive, unreinforced stimulus is by applying a Hebbian type of plasticity from the LNs onto the PNs. Even though other synaptic changes were also valid to some extent, the LN to PN connectivity changes were the most consistent in implementing filtering of frequent, repetitive information. This result corresponds to a recent report of nonassociative modification of the fruit fly AL response to carbon dioxide, which occurs at least in part because of modification of LN to PN synapses (Sachse et al., 2007). Moreover, odor–specific habituation in the fruit fly AL was recently mapped to these same synapses (Das et al, 2011). Thus our model, which was inspired by behavioral and imaging studies we reported here in the honey bee, has been validated by empirical studies in the fruit fly that identified the same type of synapse.

Furthermore, our model has gone beyond earlier studies to suggest why plasticity specifically at these synapses is the most effective way to modify the circuit. The reason that LN to PN synapses are more effective is that there is a more direct and specific connection to the PN. When a PN and LN are coactivated only that synapse becomes modified (Fig. 7A–C). Modification of a PN to LN synapse would more often equally inhibit several PNs, including ones that are not involved in the response to odor. For example, modification of the red PN to LN connection in Fig. 7A would equally change the inhibition to the blue and red PNs. Therefore, plasticity from the PN into LNs was relatively less effective because this pathway represents second-order synapses onto the PN population. The second-order nature of the connections makes it more challenging to engineer the filtering mechanism by means of local or Hebbian type learning rules, although the filtering effect may arise for some favorable asymmetric initial set of network connections.

It is conceivable that the same result, both in terms of the AL activity and behavioral conditioning, would arise if the response in activated ORNs were to decrease, for example, through some form of adaptation or Hebbian decrease in the synaptic strength of the ORN to PN connection. However, we observed no evidence of change in PN activity after odor exposure. Furthermore, this may not be an adequate means to accomplish filtering. This kind of modification would more directly, and perhaps more significantly, diminish an animal's ability to process an odor when the meaning of that odor changes. Using the indirect route that we propose would at least allow the PN to be activated, which might turn out to be an important means for reversing the plasticity when necessary. We have not extensively tested this possible model yet, at least beyond what we present in Figs 2 and 5.

We did not find any indication of changes in the spatiotemporal representation of the exposed or the novel odor as a result of unreinforced odor exposure. The correlation coefficients between the exposed and the novel odor were the same before and after conditioning. Instead, the changes induced by training became evident only in the representation of the mixture. The computational model that we implemented was useful to define that this outcome is possible under certain levels of inhibition and specific plasticity rules. The increased level of inhibition at LN to PN synapses after unrewarded exposure,

together with the higher amount of inhibition recruited by the mixture, were sufficient to inhibit PNs of the exposed odor. Alternatively, the total amount of inhibition recruited by the exposed odor alone was insufficient to inhibit the PNs activated by the exposed odor. Therefore the exposed odor could still be processed when presented alone.

The filtering effect is very relevant in the context of information processing in the brain. Stimuli that occur frequently and without direct consequences have much less information than rare ones, which may or may not have consequences (Shannon, 1948). We argue that the antennal lobe facilitates odor discrimination by reducing information that is not relevant via a Hebbian plasticity rule from the LNs to the PNs, which operates without reinforcement. It helps to reduce the importance of information that occurs too frequently and which does not have any associated positive or negative gain with it. Future studies will have to address how associative and non-associative plasticity mechanisms interact to prevent repeated but reinforced stimuli to be less represented in a mixture.

Our work, as well as other studies of plasticity in early sensory processing (Faber et al., 1999; Yu et al., 2004; Sachse et al., 2007; Daly and Smith, 2000; Das et al., 2011; Sandoz et al., 2003), raises two important questions that now need to be addressed. First, what modulatory pathway – if any - is involved in modulation of synapses to accomplish the nonassociative plasticity we have described? The computational model that we used did not implement a modulatory pathway. However, there are several possibilities for modulatory circuits. The biogenic amines octopamine and dopamine have been implicated in associative conditioning of appetitive (sucrose) and aversive (electroshock) stimuli in the honey bee and fruit fly brains (Hammer, 1997; Farooqui et al., 2003; Schwaerzel et al., 2003; Vergoz et al., 2007). It may therefore be that these or other biogenic amines are involved in nonassociative conditioning. Furthermore, NMDA receptors have been identified in the honey bee brain (Zannat et al., 2006) and have been shown to be involved in plasticity that underlies odor specific habituation in the *Drosophila* AL (Das et al., 2011). Nitric oxide is also present in insect antennal lobes and may be involved in synaptic plasticity (Müller and Hildebrandt, 2002).

The second important question regards how other areas of the brain interact with or even help drive plasticity in the AL. We have shown that the representation of the exposed odor does not change as a result of odor exposure, yet our earlier behavioral studies have shown that the behavior toward the exposed odor changes (Chandra et al., 2010). Therefore, plasticity in the AL alone cannot completely account for latent inhibition. For this reason we propose that the AL only provides an initial filtering – or preprocessing - of the signal that in some as of yet unspecified way helps downstream processing. But this raises the question of the relationship between plasticity in the AL to plasticity in other areas of the brain, and whether what we have measured even originates in the AL. Several lines of argument support the conclusion that plasticity we have identified could reside in the AL itself. Studies in the fruit fly (Sachse et al., 2007; Das et al., 2011) have shown that some components of the plasticity reside at LN to PN synapses in the AL. Furthermore, activation of different signaling pathways in the AL is crucial for different forms of olfactory memory (Grünbaum & Müller 1998; Müller, 2000; Müller & Hildebrandt 2002; Ashraf et al., 2006; Thum et al., 2007), and structural plasticity in the AL as consequence of olfactory experience has been shown in Winnington et al., 1996; Sigg et al., 1997; Devaud et al., 2001; Sachse et al., 2007; Hourcade et al., 2009 and Das et al., 2011. Finally, our model suggests that the kind of non-associative learning that we are studying here can be achieved by the sole participation of the intrinsic elements of the AL network (i.e ORNs, LNs and PNs) combined with hebbian plasticity.

However, we cannot rule out that the changes underlying plasticity in the AL could be influenced by feedback from other brain areas. Feedback neurons from the mushroom bodies to the ALs have been reported in the fruit fly (Hu et al., 2010) and honey bee (Kirschner et al., 2006 Rybak & Menzel 1993). Any feedback from the mushroom bodies to the AL that would account for the plasticity we have identified would need to be selective to provide modulation of odor specific PNs. The current anatomical description of the feedback pathway in the honey bee involves a single, or at most a few, neurons that make broad connections across glomeruli in the AL. Therefore, any modulation would seem to be broad based and lack the needed specificity to account for our data. Nevertheless, future studies should be focused at describing the specific origin and target of feedback neurons, and it will be important to establish whether the changes we observe in the AL are necessary and/or sufficient for producing the behavioral effect reported here. Indeed, changes in the visual context affect behavioral expression of latent inhibition (Chandra et al., 2010). It would be interesting to establish whether alteration of the visual context changes expression of latent inhibition in the antennal lobe, which would most likely occur via feedback.

In summary, we now know that there are subtle changes in the AL activity due to unsupervised learning that filters the most common information. Combining modeling with empirical work has benefitted our study by providing specific explanations for why the changes occur, both from a mechanistic and theoretical basis. It has provided us with several new testable hypotheses for future work. The answer to these questions will no doubt require further combined empirical and computation modeling studies.

Acknowledgments

Mathias Ditzen for providing analytical software. Funding: This research was funded by the NIH NCRR grant RR014166 to BHS, NIDCD grant DC007997 to BHS and NIDCD grant DC011422 (to RH, BHS and M Bazhenov). Grant BMBF 01GQ0771 from the German Research Ministry to CGG.

Abbreviations

AL	antennal lobe
OB	Olfactory bulb
LNs	Local Neurons
PNs	Projection Neurons
ORNs	Olfactory Receptor Neurons

REFERENCES

Abel R, Rybak J, Menzel R. Structure and response patterns of olfactory interneurons in the honeybee, Apis mellifera. J. Comp. Neurol. 2001; 437:363–383. [PubMed: 11494262]

Ashraf SI, McLoon AL, Sclarsic SM, Kunes S. Synaptic protein synthesis associated with memory is regulated by the RISC pathway in Drosophila. Cell. 2006; 124:191–205. [PubMed: 16413491]

Bazhenov M, Stopfer M, Rabinovich M, Abarbanel HD, Sejnowski TJ, Laurent G. Model of cellular and network mechanisms for odor-evoked temporal patterning in the locust antennal lobe. Neuron. 2001; 30:569–581. [PubMed: 11395015]

Bitterman ME, Menzel R, Fietz A, Schafer S. Classical conditioning of proboscis extension in honeybees (Apis mellifera). J. Comp. Psychol. 1983; 97:107–119. [PubMed: 6872507]

Chandra SB, Wright GA, Smith BH. Latent inhibition in the honey bee, Apis mellifera: Is it a unitary phenomenon? Anim. Cogn. 2010; 13:805–815. [PubMed: 20521073]

Cleland TA, Morse A, Yue EL, Linster C. Behavioral models of odor similarity. Behav. Neurosci. 2002; 116:222–231. [PubMed: 11996308]

Daly K, Christensen TA, Lei H, Smith BH, Hildebrand JG. Learning modulates the ensemble representations for odors in primary olfactory networks. Proc. Natl. Acad. Sci. U S A. 2004; 101:10476–10481. [PubMed: 15232007]

Daly KC, Smith BH. Associative olfactory learning in the moth Manduca sexta. J. Exp. Biol. 2000; 203:2025–2038. [PubMed: 10851119]

Das S, Sadanandappa MK, Dervan A, Larkin A, Lee JA, Sudhakaran IP, Priya R, Heidari R, Holohan EE, Pimentel A, Gandhi A, Ito K, Sanyal S, Wang JW, Rodrigues V, Ramaswami M. Plasticity of local GABAergic interneurons drives olfactory habituation. Proc. Nat. Acad. Sci. USA. 2011; 108:646–654.

Deisig N, Giurfa M, Lachnit H, Sandoz JC. Neural representation of olfactory mixtures in the honeybee antennal lobe. Eur.J.Neurosci. 2006; 24:1161–1174. [PubMed: 16930442]

Deisig N, Giurfa M, Sandoz JC. Antennal lobe processing increases separability of odor mixture representations in the honeybee. J.Neurophysiol. 2010; 103:2185–2194. [PubMed: 20181736]

Denker M, Finke R, Schaupp F, Grun S, Menzel R. Neural correlates of odor learning in the honeybee antennal lobe. Eur.J Neurosci. 2010; 31:119–133. [PubMed: 20104653]

Destexhe A, Mainen ZF, Sejnowski TJ. Synthesis of models for excitable membranes, synaptic transmission and neuromodulation using a common kinetic formalism. J. Comput. Neurosci. 1994; 1:195–230. [PubMed: 8792231]

Devaud JM, Acebes A, Ferrús A. Odor exposure causes central adaptation and morphological changes in selected olfactory glomeruli in Drosophila. J Neurosci. 2001; 21:6274–6282. [PubMed: 11487650]

Distler PG, Gruber C, Boeckh J. Synaptic connections between GABA-immunoreactive neurons and uniglomerular projection neurons within the antennal lobe of the cockroach, Periplaneta americana. Synapse. 1998; 29:1–13. [PubMed: 9552171]

Faber T, Joerges J, Menzel R. Associative learning modifies neural representations of odors in the insect brain. Nat. Neurosci. 1999; 2:74–78. [PubMed: 10195183]

Farooqui T, Robinson K, Vaessin H, Smith BH. Modulation of early olfactory processing by an octopaminergic reinforcement pathway in the honeybee. J. Neurosci. 2003; 23:5370–5380. [PubMed: 12832563]

Fdez. Galán R, Sachse S, Galizia CG, Herz AV. Odor-driven attractor dynamics in the antennal lobe allow for simple and rapid olfactory pattern classification. Neural. Comput. 2004; 16:999–1012. [PubMed: 15070507]

Fernandez PC, Locatelli FF, Person-Rennell N, Deleo G, Smith BH. Associative conditioning tunes transient dynamics of early olfactory processing. J. Neurosci. 2009; 29:10191–10202. [PubMed: 19692594]

Flanagan D, Mercer AR. An atlas and 3-D reconstruction of the antennal lobes in the worker honey bee, Apis mellifera (Hymenoptera, Apidae). International Journal of Insect Morphology & Embyrology. 1989; 18:145–159.

Galan RF, Weidert M, Menzel R, Herz AV, Galizia CG. Sensory memory for odors is encoded in spontaneous correlated activity between olfactory glomeruli. Neural. Comput. 2006; 18:10–25. [PubMed: 16354378]

Galizia CG, McIlwrath SL, Menzel R. A digital three-dimensional atlas of the honeybee antennal lobe based on optical sections acquired by confocal microscopy. Cell & Tissue Res. 1999; 295:383–394. [PubMed: 10022959]

Galizia, CG.; Vetter, R. Optical methods for analyzing odor-evoked activity in the insect brain. In: Christensen, TA., editor. Advances in Insect Sensory Neuroscience. Boca Raton: CRC press; 2004. p. 349-392.

Guerrieri F, Schubert M, Sandoz JC, Giurfa M. Perceptual and neural olfactory similarity in honeybees. PLoS Biol. 2005; 3(4):e60. [PubMed: 15736975]

Grünbaum L, Müller U. Induction of a specific olfactory memory leads to a long-lasting activation of protein kinase C in the antennal lobe of the honeybee. J Neurosci. 1998; 18:4384–4392. [PubMed: 9592115]

Hammer M. The neural basis of associative reward learning in honeybees. TINS. 1997; 20:245–252. [PubMed: 9185305]

Hildebrand JG, Shepherd GM. Mechanisms of olfactory discrimination: converging evidence for common principles across phyla. Annu. Rev. Neurosci. 1997; 20:595–631. [PubMed: 9056726]

Hourcade B, Perisse E, Devaud JM, Sandoz JC. Long-term memory shapes the primary olfactory center of an insect brain. Learn.Mem. 2009; 16:607–615. [PubMed: 19794186]

Hu A, Zhang W, Wang Z. Functional feedback from mushroom bodies to antennal lobes in the Drosophila olfactory pathway. Proc Natl Acad Sci U S A. 2010; 107:10262–10267. [PubMed: 20479249]

Huerta R, Sánchez-Montañés MA, Corbacho F, Sigüenza JA. A central pattern generator to control a pyloric-based system. Biol. Cybern. 2000; 82:85–94. [PubMed: 10650910]

Huerta R, Rabinovich M. Reproducible sequence generation in random neural ensembles. Phys. Rev. Lett. 2004; 93 238104.

Hunter AJ, Murray TK. Cholinergic mechanisms in a simple test of olfactory learning in the rat. Psychopharmacology (Berl). 1989; 99:270–275. [PubMed: 2508165]

Joerges J, Küttner A, Galizia CG, Menzel R. Representation of odours and odour mixtures visualized in the honeybee brain. Nature. 1997; 387:285–288.

Kirschner S, Kleineidam CJ, Zube C, Rybak J, Grünewald B, Rössler W. Dual olfactory pathway in the honeybee, *Apis mellifera*. J. Comp. Neurol. 2006; 499:933–952. [PubMed: 17072827]

Linster C, Menon AV, Singh CY, Wilson DA. Odor-specific habituation arises from interaction of afferent synaptic adaptation and intrinsic synaptic potentiation in olfactory cortex. Learn. Mem. 2009; 16:452–459. [PubMed: 19553383]

Lubow RE. Latent Inhibition. Psychological Bulletin. 1973; 79:398–407. [PubMed: 4575029]

Mauelshagen J. Neural correlates of olfactory learning paradigms in an identified neuron in the honeybee brain. J .Neurophysiol. 1993; 69:609–625. [PubMed: 8459289]

Mazor O, Laurent G. Transient dynamics versus fixed points in odor representations by locust antennal lobe projection neurons. Neuron. 2005; 48:661–673. [PubMed: 16301181]

Müller U. Prolonged activation of cAMP-dependent protein kinase during conditioning induces long-term memory in honeybees. Neuron. 2000; 27:159–168. [PubMed: 10939339]

Muller U, Hildebrandt H. Nitric oxide/cGMP-mediated protein kinase A activation in the antennal lobes plays an important role in appetitive reflex habituation in the honeybee. J. Neurosci. 2002; 22:8739–8747. [PubMed: 12351749]

Peele P, Ditzen M, Menzel R, Galizia CG. Appetitive odor learning does not change olfactory coding in a subpopulation of honeybee antennal lobe neurons. J. Comp. Physiol. A Neuroethol. Sens. Neural. Behav. Physiol. 2006; 192:1083–1103. [PubMed: 16865372]

Rath L, Galizia CG, Szyszka P. Multiple memory traces after associative learning in the honey bee antennal lobe. Eur. J. Neurosci. 2011; 34:352–360. [PubMed: 21692886]

Rybak J, Menzel R. Anatomy of the mushroom bodies in the honey bee brain: the neuronal connections of the alpha-lobe. J.Comp.Neurol. 1993; 334:444–465. [PubMed: 8376627]

Sachse S, Galizia CG. Role of inhibition for temporal and spatial odor representation in olfactory output neurons: a calcium imaging study. J. Neurophysiol. 2002; 87:1106–1117. [PubMed: 11826074]

Sachse S, Galizia CG. The coding of odour-intensity in the honeybee antennal lobe: local computation optimizes odour representation. Eur. J. Neurosci. 2003; 18:2119–2132. [PubMed: 14622173]

Sachse S, Rappert A, Galizia CG. The spatial representation of chemical structures in the antennal lobe of honeybees: steps towards the olfactory code. Eur. J. Neurosci. 1999; 11:3970–3982. [PubMed: 10583486]

Sachse S, Rueckert E, Keller A, Okada R, Tanaka NK, Ito K, Vosshall LB. Activity-dependent plasticity in an olfactory circuit. Neuron. 2007; 56:838–850. [PubMed: 18054860]

Sandoz JC, Galizia CG, Menzel R. Side-specific olfactory conditioning leads to more specific odor representation between sides but not within sides in the honeybee antennal lobes. Neuroscience. 2003; 120:1137–1148. [PubMed: 12927218]

Schwaerzel M, Monastirioti M, Scholz H, Friggi-Grelin F, Birman S, Heisenberg M. Dopamine and octopamine differentiate between aversive and appetitive olfactory memories in Drosophila. J. Neurosci. 2003; 23:10495–10502. [PubMed: 14627633]

Shannon CF. A mathematical theory of communication. Bell System Technical Journal. 1948; 27:379–423.

Sigg D, Thompson CM, Mercer AR. Activity-dependent changes to the brain and behavior of the honey bee, Apis mellifera (L.). J Neurosci. 1997; 17:7148–7156. [PubMed: 9278549]

Smith BH. The role of attention in learning about odorants. Biol. Bull. 1996; 191:76–83. [PubMed: 8776843]

Smith BH. Analysis of interaction in binary odorant mixtures. Physiol. Behav. 1998; 65:397–407. [PubMed: 9877404]

Smith, BH.; Wright, GA.; Daly, KS. Learning-based recognition and discrimination of floral odors. In: Dudareva, N.; Pichersky, E., editors. The Biology of Floral Scents. Boca Raton, FL: CRC Press; 2006. p. 263-295.

Stopfer M, Laurent G. Short-term memory in olfactory network dynamics. Nature. 1999; 402:664–668. [PubMed: 10604472]

Strausfeld NJ, Hildebrand JG. Olfactory systems: common design, uncommon origins? Curr. Opin. Neurobiol. 1999; 9:634–639. [PubMed: 10508748]

Szücs A, Huerta R, Rabinovich MI, Selverston AI. Robust microcircuit synchronization by inhibitory connections. Neuron. 2009; 61:439–453. [PubMed: 19217380]

Thum AS, Jenett A, Ito K, Heisenberg M, Tanimoto H. Multiple memory traces for olfactory reward learning in Drosophila. J Neurosci. 2007; 27:11132–11138. [PubMed: 17928455]

Vergoz V, Roussel E, Sandoz JC, Giurfa M. Aversive learning in honeybees revealed by the olfactory conditioning of the sting extension reflex. PLoS One. 2007; 2:e288. [PubMed: 17372627]

Wilson RI, Turner GC, Laurent G. Transformation of olfactory representations in the Drosophila antennal lobe. Science. 2004; 303:366–370. [PubMed: 14684826]

Wilson HR, Cowan RD. Excitatory and Inhibitory interactions in localized populations of model neurons. J. Biophys. 1972; 12:1–24.

Wilson DA, Linster C. Neurobiology of a simple memory. J. Neurophysiol. 2008; 100:2–7. [PubMed: 18463176]

Winnington AP, Napper RM, Mercer AR. Structural plasticity of identified glomeruli in the antennal lobes of the adult worker honey bee. J Comp Neurol. 1996; 365:479–490. [PubMed: 8822183]

Yu D, Ponomarev A, Davis RL. Altered representation of the spatial code for odors after olfactory classical conditioning; memory trace formation by synaptic recruitment. Neuron. 2004; 42:437–449. [PubMed: 15134640]

Zannat MT, Locatelli F, Rybak J, Menzel R, Leboulle G. Identification and localisation of the NR1 sub-unit homologue of the NMDA glutamate receptor in the honeybee brain. Neurosci. Lett. 2006; 398:274–279. [PubMed: 16480817]

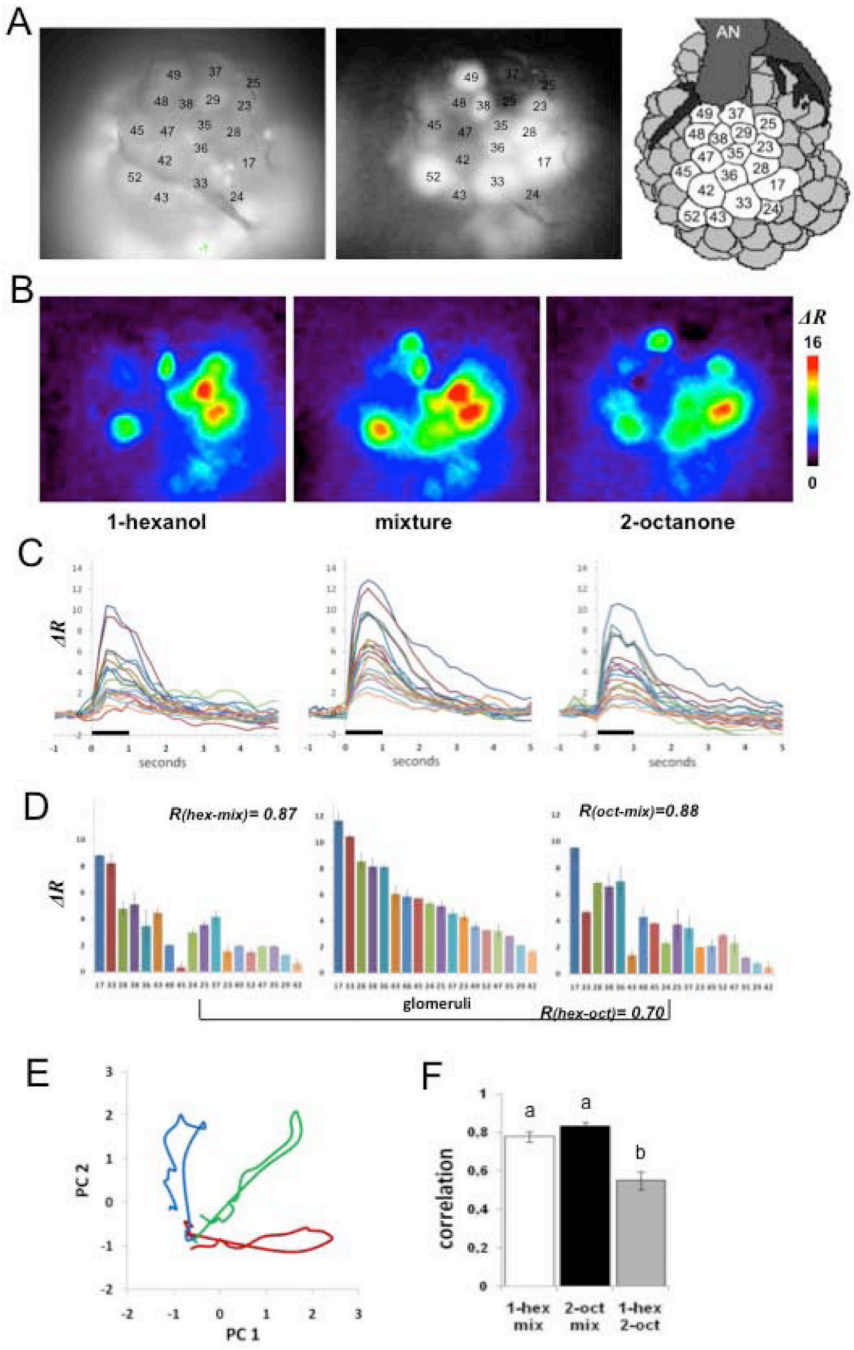

Figure 1.

Calcium imaging of projection neurons in the honey bee antennal lobe. ***A,*** View of the antennal lobe after staining the PNs. The picture shows the dorsal surface including 18 identified glomeruli (Galizia et al., 1999) used for the imaging analyses. *Left:* basal fluorescence images obtained with 380nM excitation light and LP510 emission filter, allow identification of glomeruli according to size, shape and position by comparison with the published honey bee AL atlas (Galizia et al., 1999; Flanagan and Mercer 1989). Basal fluorescence images are also used for verification of homogeneous staining in all glomeruli used for analysis. *Middle panel:* Correlation images (see methods) clearly define boundaries between glomeruli and thus were used as an additional tool to verify glomeruli

identification. Darker glomeruli do not indicate lack of staining (controlled for from the images such as the one in the left panel); these glomeruli were not activated by the odors and consequently produce a low correlation values between neighboring pixels). *Right panel*: Schema of the dorsal surface on the honey bee AL showing 18 glomeruli used in our analyses (AN: antennal nerve). ***B***, Color-coded (see scale) changes in calcium levels averaged between 400 and 800 ms after odor onset. The figures show distinct but slightly overlapping spatial activity patterns for each of the three odors. ***C,*** Glomerular activity over time to show spatio-temporal activity patterns. The same line color across figures represents the change in ratio over 6 s (1 s before stimulation through 5 s after) in a single identified glomerulus for each of the three odors. ***D,*** Calcium responses for each of the 18 glomeruli averaged over 1s of stimulation ordered from the highest response to the lowest for the mixture (middle figure). The same ordering was maintained for 1-hexanol (left) and 2-octanone (right) to emphasize changes in activity in each glomerulus for each of the odors compared to the mixture. Error bars represent Standard Deviation of two measurements. R-values inserted in the Fig. 1D refer to the Pearson correlation coefficients used to compare pairs of odor patterns within animal and within session. ***E***, Principal Components Analysis (see Methods) used to show the evolution of the activity patterns over 200 ms time steps during odor stimulation in one animal (Galan et al., 2006; Fernandez et al., 2009) for 1-hexanol (blue), the mixture (green) and 2-octanone (red). With the onset of odor stimulation the transients for the pure odors project along each PC axis and reach maximal separation between 400 and 600 ms (Fernandez et al., 2009). After odor termination the transients loop back and return to origin. ***F***, Mean +/− SE of the correlation coefficients indicated in D, for 17 animals prior to any treatment. The correlations between the pure components and the mixture are significantly higher than the correlation between the pure odorants; different letters on tops of the bars indicate significant differences at $p<0.01$.

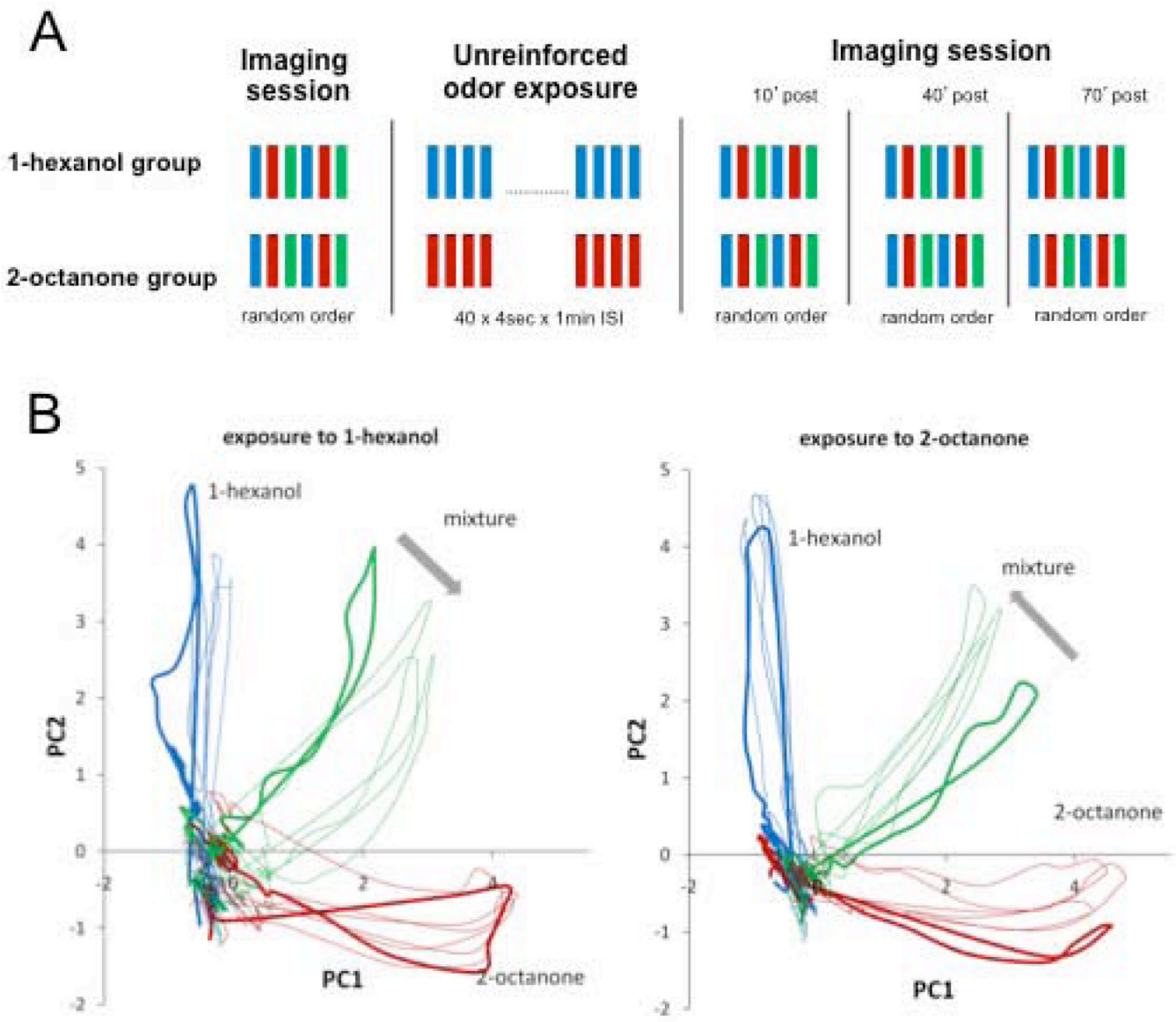

Figure 2.

Effect of odor exposure on odor-induced spatiotemporal activity in the AL. ***A***, Experimental protocol: Each imaging session includes two stimulations each with 1-hexanol, 2-octanone and the mixture (1:1) distributed in random order and separated by 1min ISI. The exposure consisted of 40 4-sec presentations of either 1-hexanol or 2-octanone separated by 1 min inter-stimulus interval (ISI). The exposure session started 5 min after the end of the first imaging session. Odor representations were measured again in the second, third and fourth imaging session performed 10, 40 and 70 minutes after the end of the exposure, respectively. ***B***, Odor elicited responses from 18 glomeruli are represented using Principal Component Analysis. The animals exposed to 1-hexanol (n=8) and to 2-octanone (n=9) were separately averaged to obtain two average-bees with 18 glomeruli each (Methods; Fernandez et al 2009). The 18 dimensions used to describe odor transients were reduced to its first two principal components (95% and 97 % of the total variance respectively). Bold lines indicate the first imaging session, which was done before the exposure session. Thin lines belong to the 2^{nd}, 3^{rd} and 4^{th} imaging sessions performed after exposure. We use PCA for

visualization only. Statistical analyses as well as conclusions are based on the absolute correlation values presented in figure 3.

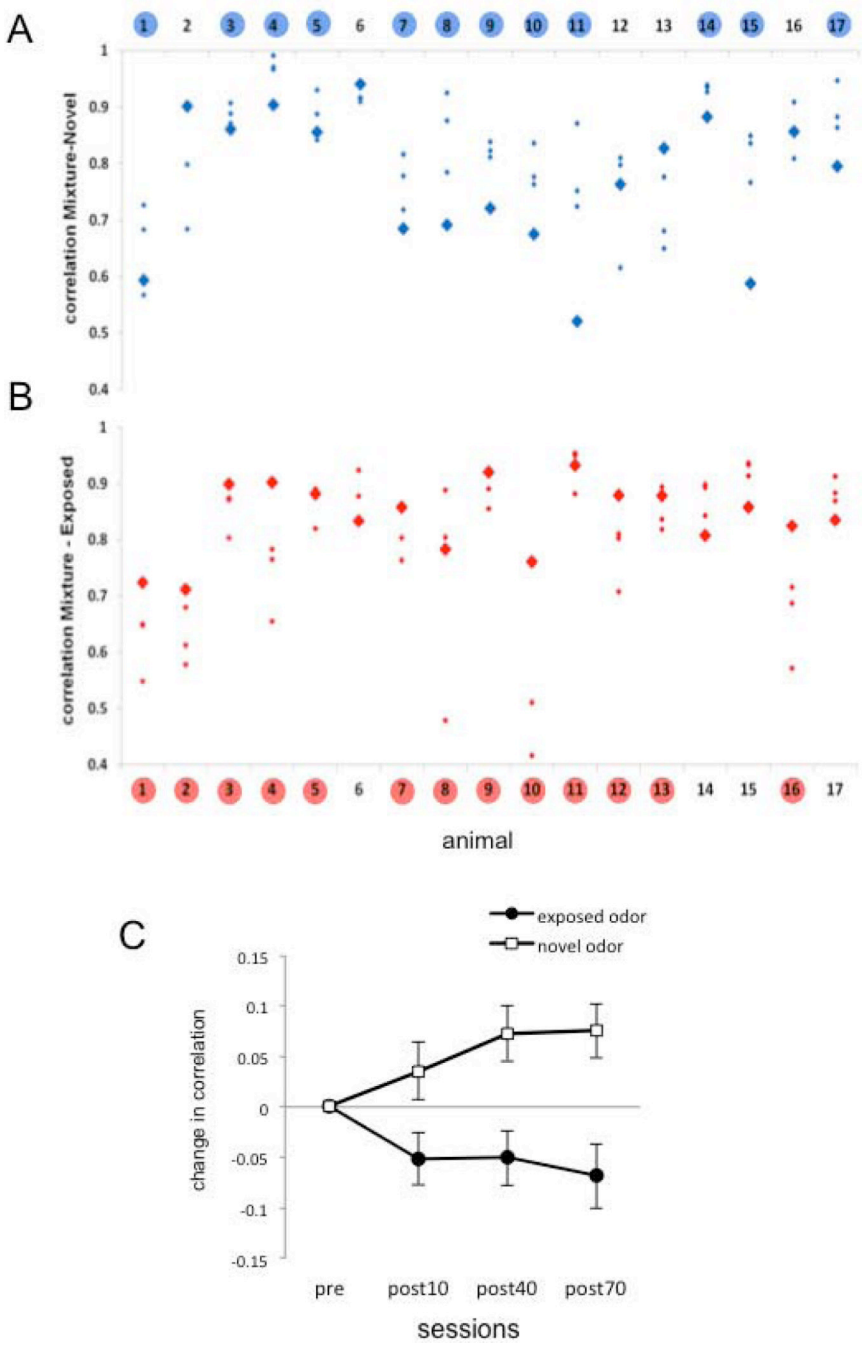

Figure 3.

Correlation coefficients between the mixture and the pure odors before and after exposure. ***A.*** Absolute Pearson correlation coefficients between the activity patterns elicited by the novel odor (odor not used during exposure) and the mixture for each individual bee (n=17). Bold blue diamonds correspond to the correlation value before exposure. Small diamonds correspond to the correlation values after exposure. Numbers highlighted in blue indicate bees in which the average of the correlation from the three post-exposure sessions is higher than the correlation in the initial session. ***B***. Absolute Pearson correlation coefficients between the exposed odor and the mixture for each individual bee. Bold red diamonds

correspond to the measurement performed before exposure and small diamonds to the measurements performed after exposure. Numbers highlighted in red indicate bees in which the average of the correlation values obtained in the three post-exposure sessions is lower than the correlation in the initial session. Statistical analysis was strictly based on raw correlation values as they are shown in figures A and B. Two factors repeated measures ANOVA; factor 1 “novel or exposed” odor, NS; factor 2 (repeated measurement) “sessions”, NS; Interaction p =0.001. ***C.*** The data from figures A and B plotted as the net change of the correlation along the experiment. The figure shows the average and SEM of the difference between each post-exposure session and the session before exposure (n=17). The change in correlation was calculated within each bee by subtracting the correlation value obtained in the first test session from the values obtained in the post-exposure sessions.

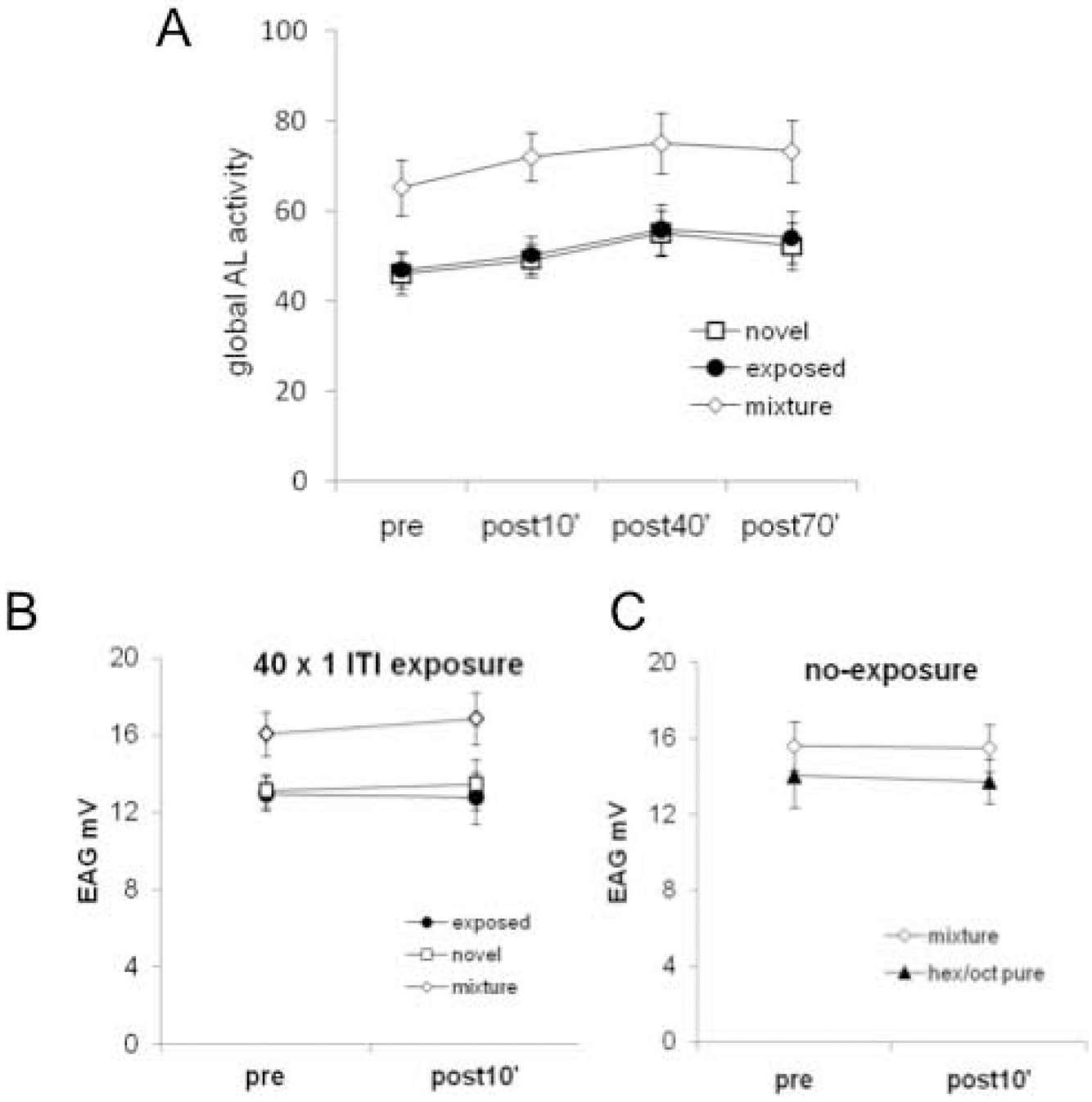

Figure 4.

Evaluation of sensory adaptation as a possible basis for the effect in the antennal lobe. ***A***. Global antennal lobe activity elicited by the exposed odor, the novel odor and the mixture along all sessions. The figure shows the sum of the calcium responses in the 18 measured glomeruli. No differences were found for 1-hexanol or 2-octanone exposed bees (data not shown). Data were therefore pooled for the exposed odor, novel odor or mixture and analyzed along sessions. Statistical significance $p<0.01$ for both pure odors against the mixture and $p<0.01$first session against the third, and between fourth sessions for all odors; interaction not significant. The differences reported along sessions were not specific for the

exposed odor. ***B.*** EAG was performed for the mixture and the pure odors 10’ before and 10’ after the exposure protocol coincident in time with the first and second session of the imaging experiments. Responses pre- vs post- were not significantly different (n=10 bees). ***C,*** A group of animals underwent two EAG sessions separated by 60 min, with no exposure protocol in-between, but coincident in time with the first and the second session of the imaging experiment. No change between both sessions was observed (n=5 bees).

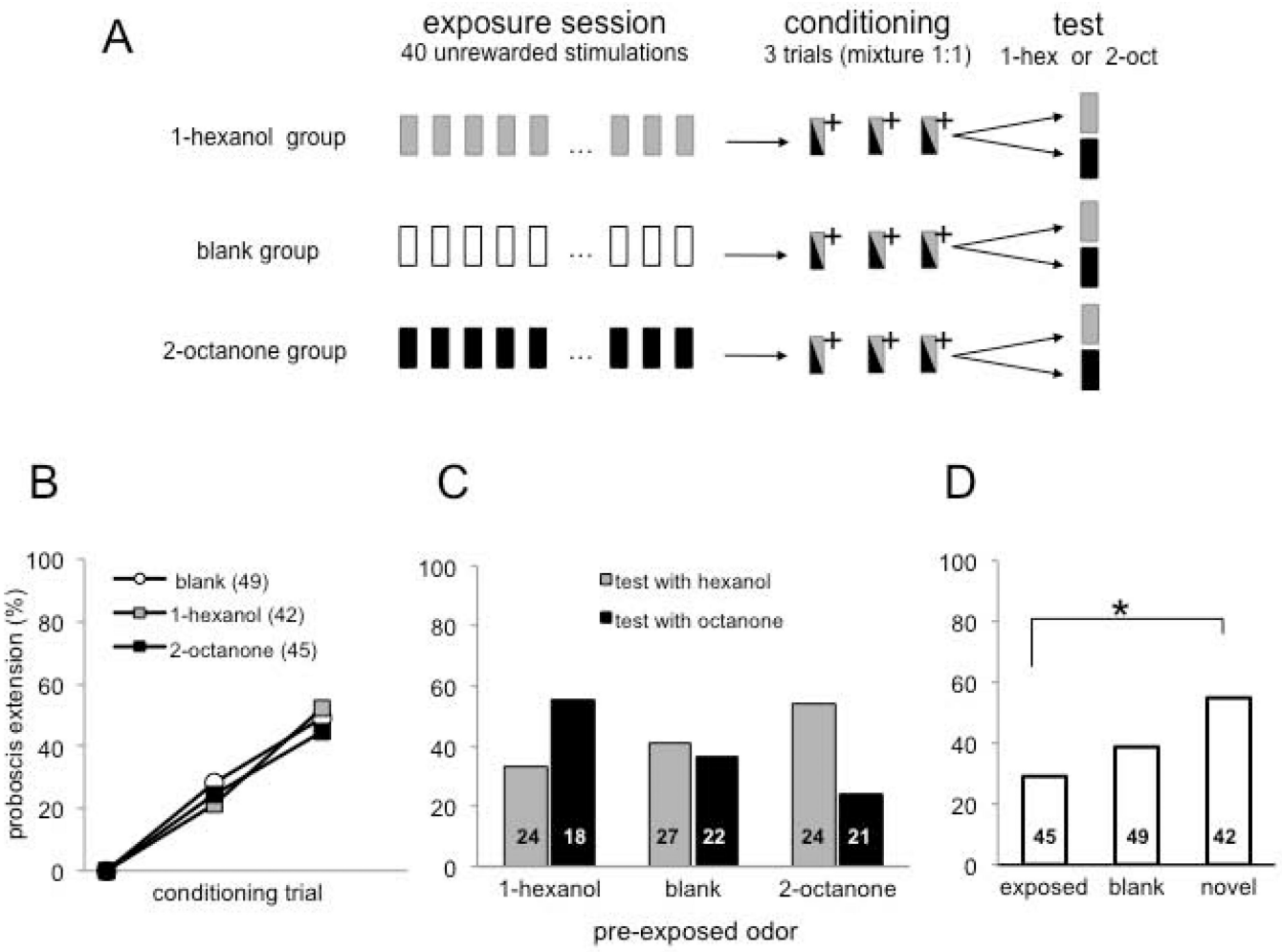

Figure 5.

Effect of repeated odor exposure on perception of an odor mixture. ***A***, Schema showing the experimental procedure. *Exposure session*: 40 unrewarded stimulations with 1-hexanol, 2-octanone or air (blank group); *Conditioning session*: olfactory conditioning of the proboscis extension reflex (Bitterman et al., 1983) using a 1:1 mixture (1-hexanol: 2-octanone); (+) indicates reinforcement with 0.4 μl of 2M sucrose paired with the mixture. *Test session*: conditioned response was tested with 1-hexanol or 2-octanone (animals were tested only once). Proboscis extension response during exposure protocol was not recorded, since these two odors do normally not elicit any response before conditioning. ***B***, Performance during conditioning showing percentage of animals extending the proboscis to the mixture during the three training trials. Results indicate % of response during the odor period and before reward. All groups were trained identically; they differed only in regard to treatment during the exposure session before training. No difference was found for the three groups and significant effect between trials for all groups. ***C***, Each of the three groups was split into 2 groups for testing with the pure components (1-hexanol or 2-octanone). Two-way ANOVA revealed a significant interaction between exposed odor (1-hexanol, 2-ocatanone or air) and test odor $F_{(2,130)}= 3.09$ $p<0.05$. Numbers in the bars indicate number of animals in each test condition in each exposure group. ***D***, Same data from C reorganized by *exposed odor* (1-hexanol and 2-octanone as test odors when animals had been exposed to 1-hexanol or 2-octanone, respectively); *novel odor* (1-hexanol and 2-octanone as test odors when animals

had been exposed to 2-octanone or to 1-hexanol, respectively); or *blank* (1-hexanol and 2-octanone as test odors after exposure to air). ***** $p<0.05$ between exposed and novel odors.

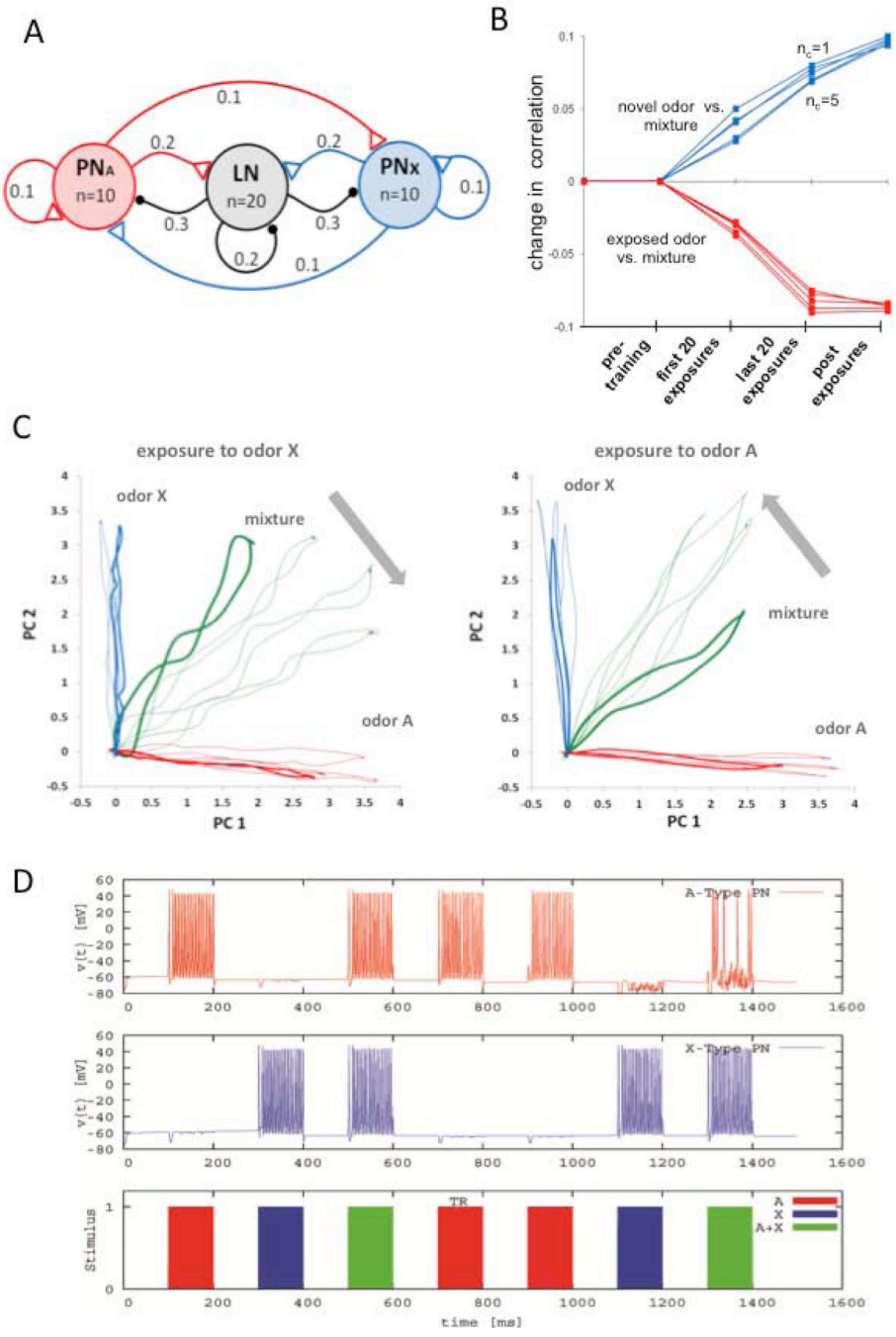

Figure 6.

Hebbian plasticity on LN-to-PN synapses predicts the imaging results. ***A***, Model of the antennal lobe topology used in the computational analyses. The network consists of 20 inhibitory local interneurons (LNs) and 20 projection neurons (PNs). This population is illustrated as three clusters in the figure. The connectivity within and between the clusters is determined randomly, based on the fixed probabilities indicated on the links. Connectivity probabilities relate to individual neurons, i.e. each PN has a probability of 0.2 of connecting any neuron from the LN cluster, thus in our model each PN cluster makes approx. 40 excitatory synapses onto LNs. The synaptic conductance for each type of connection is

drawn from a normal distribution (by allowing no negative conductance). The mean and the SD of these parameters were 0.1μS and 0.05 μS for within- or between-cluster synapses and 10μS and 5μS for the external stimulation. A particular odorant reaches 10 PNs. Different degrees of overlap in the representation for A and X was evaluated by introducing from 1 to 5 common PNs (not shown in the schema). A pure odor is presented by injecting current into the set of PNs corresponding to odor A or odor X; the mixture is applied to the network by applying current in both A and X. ***B***, Change in correlation between the trajectories for the pure odors and the mixture before, during and after exposure training. The correlation is performed among ten samples (i.e., ten loops on the 2D PC plane) obtained for each category (i.e., odor A vs. mixture, and odor X vs. the mixture) and for increasing levels of overlap between odor A and odor X ranging from 1 to 5 common PNs. ***C***, The projections of the calcium trajectories of the PNs were obtained from the simulation of the computational model where each unit (PN or LN) was expressed by a conductance-based Hudgkin-Huxley-type single-compartment model. The training was performed on the same network for both odor types. In line with the experimental protocol, the affected synaptic conductances were increased to 150% of their original values in 20 odor presentations during training. ***D***, The model's prediction of the membrane potential time traces for two arbitrary PNs, one from each response group. In this instance, the training is performed with odor A and all plasticity is encapsulated in the odor presentation labeled by TR.

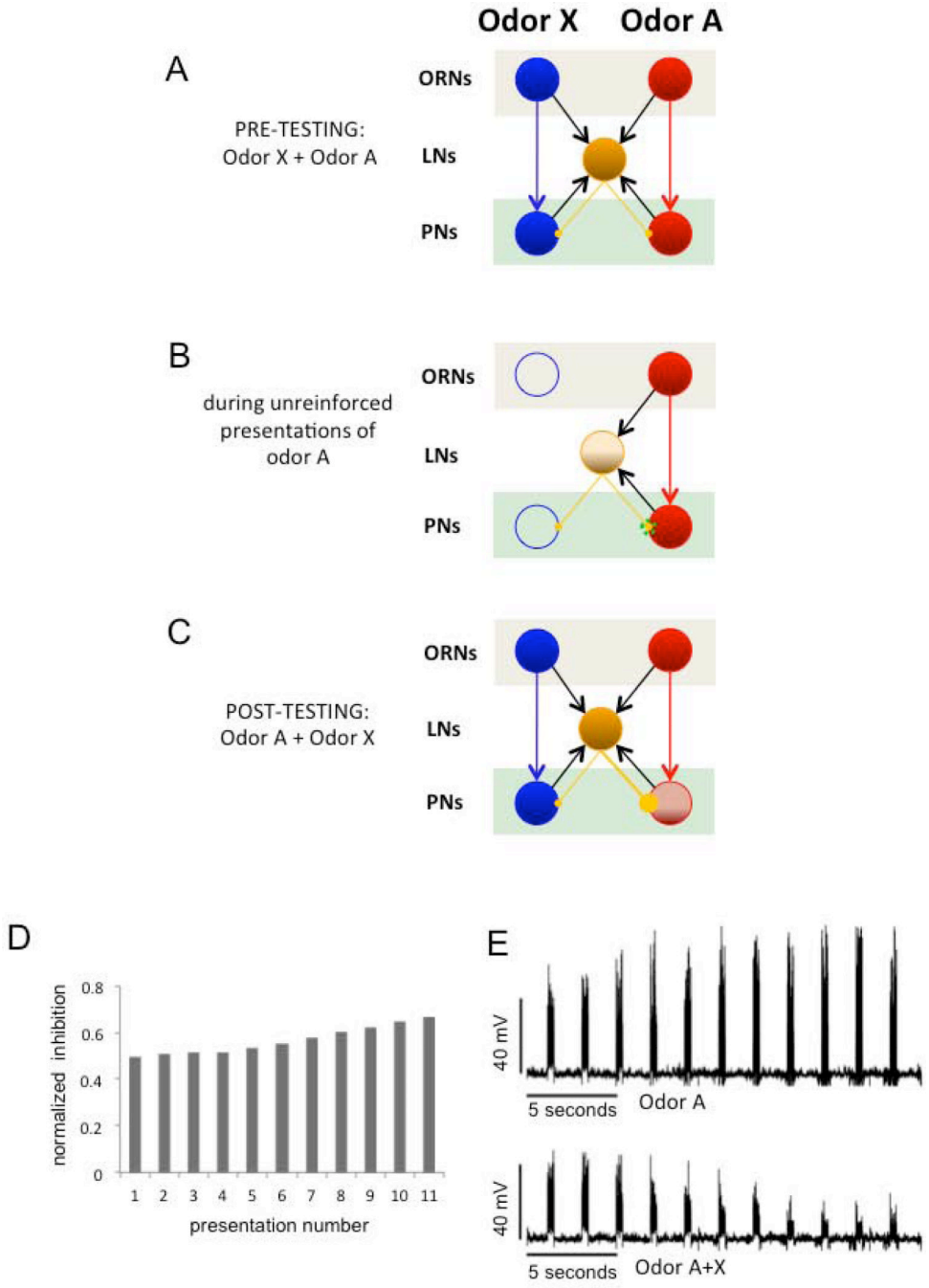

Figure 7.

Illustration of the simplest and most efficient mechanism for implementing filtering of uninformative odors in the AL. The schema indicates excitatory connections from ORNs to PNs and to LNs, excitatory connections PNs to LN and inhibitory connections from LNs to PNs. ***A***, Initially, lateral inhibition is weak and symmetric. The LN (yellow) receives input from both ORNs clusters. Since inhibitory connections are symmetric, the mixture induces a balanced representation of A and X across PNs. ***B***, Hebbian potentiation of inhibitory synapses during odor exposure. During training the connections from the LN to the PNs that are simultaneously active increase their synaptic strength. ***C***, the LN receives input from

both ORNs clusters and the inhibitory connection with PN-A was potentiated. When the odor mixture A+X is presented, the PNs responding to A become silent due to the increase of the overall inhibition arriving into those PNs as a result of training. As consequence, the blue (X) odor is more strongly represented in the pattern elicited by the mixture. In other words, odor A+X recruits a higher level of synaptic inhibition into the group A than group X. ***D***, The fraction of total inhibition on the odor-A PN group versus the total inhibition in the system after consecutive odor A presentations in B. ***E***, Average membrane potential of the odor A PN population for several presentations of that odor. The upper figure is the response when only odor A is presented. The lower figure shows the diminishing response in the same A group during successive presentations of the A+X mixture.